Electronic Supplementary Information

Role of Simultaneous Thermodynamic and Kinetic Variables in Optimizing Blade-Coated Organic Solar Cells

Yongjoon Cho,[a,c,‡] Byoungkyu Lee,[a,d,‡] Sungwoo Jung,[a] Seonghun Jeong,[a] Jeewon Park,[a] Geunhyung Park,[a] Sangjin Yang,[a] Changduk Yang[a,b,*]

[a]School of Energy and Chemical Engineering, Perovtronics Research Center, Low Dimensional Carbon Materials Center, Ulsan National Institute of Science and Technology (UNIST), 50 UNIST-gil, Ulju-gun, Ulsan 44919, South Korea

[b]Graduate School of Carbon Neutrality, Ulsan National Institute of Science and Technology (UNIST), 50 UNIST-gil, Ulju-gun, Ulsan 44919, South Korea.

[c]Department of Chemistry and Materials Research Center, Northwestern University, 2145 Sheridan Road, Evanston, IL 60208, USA

[d]Department of Physics and Organic and Carbon Electronics Laboratories (ORaCEL), North Carolina State University, Raleigh, NC 27695, USA

[‡]Y. C and B. L contributed equally to this work.

Experimental Section

Materials and instruments

ITO was purchased from Omniscience and the resistance of ITO is 9 Ω/sq. 6-ethylthieno[3,2-*b*]thiophen-2-yl)trimethylstannane (**1a**), 6-hexylthieno[3,2-*b*]thiophen-2-yl)trimethylstannane (**1b**), 6-octylthieno[3,2-*b*]thiophen-2-yl)trimethylstannane (**1c**), 6-undecylthieno[3,2-*b*]thiophen-2-yl)trimethylstannane (**1d**), and 4,7-dibromo-2-(2-ethylhexyl)-5,6-dinitro-2*H*-benzo[*d*][1,2,3]triazole (**2**) were synthesized according to the reported method.[1, 2] All the chemicals and reagents were purchased from Sigma-Aldrich, Tokyo Chemical Industry Co., Ltd, and Alfa Aesar Chemical Company and used without any further purification, and 2-(5,6-difluoro-3-oxo-2,3-dihydro-1*H*-inden-1-ylidene)malononitrile (2FIC, **6**) was purchased from SunaTech Inc. All solvents are ACS and anhydrous grade by distillation. ^{1}H NMR and ^{13}C NMR spectra of the NFAs were recorded on a Bruker AVANCE III HD 400 MHz spectrometer using deuterated CDCl$_3$ as solvent and tetramethylsilane (TMS) as an internal standard. High resolution mass spectrometry (HRMS) spectra were measured using AccuTOF 4G+ DART. UV–Vis absorption spectra of the NFAs in CF and CB solution, and film were measured by spectrophotometer (8453, Agilent Technologies). The optical bandgaps were estimated from the absorption onset of the as-cast thin films. Solubility tests of NFAs were conducted using a UV-Vis spectrophotometer (8453, Agilent Technologies). Standard NFA solutions in CF and CB at known concentrations were prepared. Then, the solutions were diluted to achieve an appropriate optical density for absorption measurements, measuring the λ_{max} values of the diluted solutions. Finally, the λ_{max} of the diluted solution from a saturated solution was compared with the calibrated linear-fit curves to quantify the solubilities using the Beer–Lambert law. DFT calculations were performed using the Gaussian 09 package at B3LYP function and the 6-31G+** basis set. CV measurements were performed on an Iviumstat.h with a three-electrode cell system in a nitrogen bubbled 0.1 M tetra-*n*-butylammonium hexafluorophosphate (n-Bu4NPF6) solution in acetonitrile at a scan rate of 100 mV^{-1} s^{-1} at room temperature. An Ag/Ag$^+$ electrode, platinum wire, and material-coated glassy carbon electrode were used as the reference electrode, counter electrode, and working electrode, respectively. The Ag/Ag$^+$ reference electrode was calibrated using a Fc/Fc$^+$ redox couple as an internal standard, whose oxidation potential was set at −4.8 eV with respect to the zero-vacuum level. HOMO and LUMO energy levels of NFAs were obtained from the equation HOMO (eV) = −(E$_{ox}^{onset}$ − E$_{Fc}^{onset}$ + 4.8) and LUMO (eV) = −(E$_{red}^{onset}$ − E$_{Fc}^{onset}$ + 4.8). The TGA curves were evaluated with a Q500 (TA Instruments, a scan rate of 5°C min^{-1}) and the DSC

measurements were conducted with DSC 4000 (PerkinElmer, a scan rate of 5°C min^{-1}). The PL analysis was performed using ELCT-3010 PL mode (Enlitech). The PL spectra under short-circuit conditions were measured from full stack devices under short-circuit conditions, with excitation at 720 nm. AFM images of thin films were obtained using multimode V microscope (Veeco, USA) with a nanoscope controller using Si tips (Bruker) and TEM analysis was performed using a JEOL USA JEM-2100F (Cs corrector) transmission electron microscope. Grazing incidence wide-angle X-ray scattering (GIWAXS) measurement was conducted at the PLS-II 9A beamline of the Pohang Accelerator Laboratory in Korea. The X-rays coming from the in-vacuum undulator were monochromated (λ = 1.10994 Å) using a double crystal monochromator and focused both horizontally and vertically (450 (H) × 60 (V) μm^2 in FWHM (full width at half maximum) @ the sample position) using K–B type mirrors. The GIWAXS sample stage was equipped with a 7-axis motorized stage for the fine alignment of the sample, and the incidence angle of the X-ray beam was set to be 0.12° for the neat and blend films. The GIXD patterns were recorded with a 2D CCD detector (Rayonix SX165) and the X-ray irradiation time was 5–30 s, dependent on the saturation level of the detector. Diffraction angles were calibrated using a sucrose standard (monoclinic, P21, a = 10.8631 Å, b = 8.7044 Å, c = 7.7624 Å, and β = 102.938°) and the sample-to-detector distance was ≈231 mm. CCL was calculated according to the following Scherrer equation: CCL = $2\pi K/\Delta q$

In this equation, CCL is the crystal coherence length, K is a shape factor (0.9), and Δq is the FWHM of a diffraction peak.

Material synthesis and characterization

Synthesis of (2-(2-ethylhexyl)-4,7-bis(6-ethylthieno[3,2-b]thiophen-2-yl)-5,6-dinitro-2H-benzo[d][1,2,3]triazole) (**3a**).

To a two-neck round-bottom flask of compounds **1a** (2.0 g, 6.02 mmol), **2** (1.2 g, 2.50 mmol), and tetrakis(triphenylphosphine)palladium(0) (0.29g, 0.250 mmol) in toluene (40 mL) were added under argon protection. The reaction mixture was refluxed overnight with vigorous stirring. After cooling to room temperature, the solvent was removed under reduced pressure. The crude was purified by column chromatography on silica gel using hexane and dichloromethane to afford the orange solid (1.42 g, 87%). ^{1}H NMR (CDCl$_3$, 400 MHz) δ ppm 7.74 (s, 2H), 7.16 (s, 2H), 4.77 (d, J = 6.8 Hz, 2H), 2.81 (qd, J = 7.5, 1.1 Hz, 4H), 2.25 (m, 1H), 1.43−1.24 (m, 14H), 1.01−0.85 (m, 6H).

Synthesis of (2-(2-ethylhexyl)-4,7-bis(6-hexylthieno[3,2-b]thiophen-2-yl)-5,6-dinitro-2H-

benzo[d][1,2,3]triazole) (**3b**).

3b was synthesized through the same synthetic route as **3a**, and **1b** (2.3 g, 6.02 mmol) was used instead of **1a**, affording the orange solid (1.73 g, 90%). ^{1}H NMR (CDCl$_3$, 400 MHz) δ ppm 7.73 (s, 2H), 7.14 (s, 2H), 4.77 (d, J = 6.8 Hz, 2H), 2.77 (m, 4H), 2.25 (m, 1H), 1.86−1.74 (m, 4H), 1.48−1.24 (m, 20H), 1.02−0.84 (m, 12H).

Synthesis of (2-(2-ethylhexyl)-5,6-dinitro-4,7-bis(6-octylthieno[3,2-b]thiophen-2-yl)-2H-benzo[d][1,2,3]triazole) (**3c**).

3c was synthesized through the same synthetic route as **3a**, and **1c** (2.5 g, 6.02 mmol) was used instead of **1a**, affording the orange solid (1.79 g, 88%). ^{1}H NMR (CDCl$_3$, 400 MHz) δ ppm 7.74 (s, 2H), 7.14 (s, 2H), 4.77 (d, J = 6.8 Hz, 2H), 2.76 (m, 4H), 2.25 (m, 1H), 1.82−1.75 (m, 4H), 1.46−1.24 (m, 28H), 1.01−0.85 (m, 12H).

Synthesis of (2-(2-ethylhexyl)-5,6-dinitro-4,7-bis(6-undecylthieno[3,2-b]thiophen-2-yl)-2H-benzo[d][1,2,3]triazole) (**3d**).

3d was synthesized through the same synthetic route as **3a**, and **1d** (2.8 g, 6.02 mmol) was used instead of **1a**, affording the orange solid (2.06 g, 91%). ^{1}H NMR (CDCl$_3$, 400 MHz) δ ppm 7.74 (s, 2H), 7.14 (s, 2H), 4.77 (d, J = 6.8Hz, 2H), 2.77 (m, 4H), 2.24 (m, 1H), 1.83−1.73 (m, 4H), 1.46−1.20 (m, 40H), 1.02−0.83 (m, 12H).

Synthesis of (3,9-diethyl-6,12,13-tris(2-ethylhexyl)-12,13-dihydro-6H-thieno[2'',3'':4',5']thieno[2',3':4,5]pyrrolo[3,2-g]thieno[2',3':4,5]thieno[3,2-b][1,2,3]triazolo[4,5-e]indole) (**4a**).

In a two-neck round-bottom flask, compound **3a** (0.50g, 0.772 mmol) and triethyl phosphite (6 mL) were dissolved in *o*-dichlorobenzene (6 mL) under argon protection. After being stirred at 180℃ overnight, the reaction mixture was cooled to room temperature and extracted with dichloromethane. The organic layer was dried over magnesium sulfate and the solvent was removed under reduced pressure. The obtained product was added into a two-neck round-bottom flask. The potassium carbonate (0.53 g, 3.86 mmol), potassium iodide (0.64 g, 3.86 mmol), 1-bromo-2-ethylhexane (0.60 g, 3.09 mmol), and dimethylformamide (20 mL) were added and the mixture was refluxed at 130℃ overnight under argon protection. Then, the reaction mixture was quenched by water and extracted with dichloromethane. The organic layer was dried over magnesium sulfate and the solvent was removed under reduced pressure. The residue was purified by column chromatography on silica gel using hexane and dichloromethane as an eluent to afford the yellow solid (0.26 g, 42%). ^{1}H NMR (CDCl$_3$, 400 MHz) δ ppm 6.99 (s, 2H), 4.72 (d, J = 7.2 Hz, 2H), 4.58 (d, J = 7.7 Hz, 4H), 2.86 (q, J = 7.5

Hz, 4H), 2.38 (m, 1H), 1.97 (m, 2H), 1.51−0.71 (m, 36H), 0.66−0.48 (m, 12H).

Synthesis of (6,12,13-tris(2-ethylhexyl)-3,9-dihexyl-12,13-dihydro-6H-thieno[2'',3'':4',5']thieno[2',3':4,5]pyrrolo[3,2-g]thieno[2',3':4,5]thieno[3,2-b][1,2,3]triazolo[4,5-e]indole) (**4b**).

4b was synthesized through the same synthetic route as **4a**, and **3b** (0.59g, 0.772 mmol) was used instead of **3a**, affording the yellow solid (0.30 g, 45%). ^{1}H NMR (CDCl$_3$, 400 MHz) δ ppm 6.98 (s, 2H), 4.72 (d, J = 7.2 Hz, 2H), 4.58 (d, J = 7.8 Hz, 4H), 2.82 (t, J = 7.7 Hz, 4H), 2.38 (m, 1H), 1.97 (m, 2H), 1.85 (m, 4H), 1.48−0.72 (m, 48H), 0.65−0.50 (m, 12H).

Synthesis of (6,12,13-tris(2-ethylhexyl)-3,9-dioctyl-12,13-dihydro-6H-thieno[2'',3'':4',5']thieno[2',3':4,5]pyrrolo[3,2-g]thieno[2',3':4,5]thieno[3,2-b][1,2,3]triazolo[4,5-e]indole) (**4c**).

4c was synthesized through the same synthetic route as **4a**, and **3c** (0.63g, 0.772 mmol) was used instead of **3a**, affording the yellow solid (0.36 g, 47%). ^{1}H NMR (CDCl$_3$, 400 MHz) δ ppm 6.98 (s, 2H), 4.72 (d, J = 7.2 Hz, 2H), 4.58 (d, J = 7.8 Hz, 4H), 2.82 (t, J = 7.7 Hz, 4H), 2.37 (m, 1H), 1.98 (m, 2H), 1.86 (m, 4H), 1.49−0.72 (m, 56H), 0.64−0.51 (m, 12H).

Synthesis of (6,12,13-tris(2-ethylhexyl)-3,9-diundecyl-12,13-dihydro-6H-thieno[2'',3'':4',5']thieno[2',3':4,5]pyrrolo[3,2-g]thieno[2',3':4,5]thieno[3,2-b][1,2,3]triazolo[4,5-e]indole) (**4d**).

4d was synthesized through the same synthetic route as **4a**, and **3d** (0.70g, 0.772 mmol) was used instead of **3a**, affording the yellow solid (0.35 g, 43%). ^{1}H NMR (CDCl$_3$, 400 MHz) δ ppm 6.98 (s, 2H), 4.72 (d, J = 7.2 Hz, 2H), 4.58 (d, J = 7.8 Hz, 4H), 2.81 (t, J = 7.7 Hz, 4H), 2.38 (m, 1H), 1.97 (m, 2H), 1.86 (m, 4H), 1.49−0.72 (m, 68H), 0.66−0.50 (m, 12H).

Synthesis of (3,9-diethyl-6,12,13-tris(2-ethylhexyl)-12,13-dihydro-6H-thieno[2'',3'':4',5']thieno[2',3':4,5]pyrrolo[3,2-g]thieno[2',3':4,5]thieno[3,2-b][1,2,3]triazolo[4,5-e]indole-2,10-dicarbaldehyde) (**5a**).

To a two-neck round-bottom flask, dimethylformamide (1 mL) and phosphorus oxychloride (1.2 mL) were added. Then dichloroethane (2 mL) was added to the mixture and stirred at room temperature for an hour. The reaction mixture was transferred dropwise into the two-neck round-bottom flask of solution of **4a** (0.12g, 0.150 mmol) in dichloroethane (10 mL) and stirred at 110°C overnight under argon protection. The reaction mixture was quenched with saturated sodium bicarbonate solution and extracted with dichloromethane. The organic layer was dried over magnesium sulfate and the solvent was removed under reduced pressure. The crude was purified by column chromatography on silica gel by using hexane and dichloromethane as an

eluent to afford the orange solid (0.12 g, 92%). ^{1}H NMR (CDCl$_3$, 400 MHz) δ ppm 10.14 (s, 2H), 4.73 (d, J = 7.2 Hz, 2H), 4.61 (d, J = 7.8 Hz, 4H), 3.24 (q, J = 7.6 Hz, 4H), 2.36 (m, 1H), 1.92 (m, 2H), 1.51−0.72 (m, 36H), 0.67−0.51 (m, 12H).

Synthesis of (6,12,13-tris(2-ethylhexyl)-3,9-dihexyl-12,13-dihydro-6H-thieno[2'',3'':4',5']thieno[2',3':4,5]pyrrolo[3,2-g]thieno[2',3':4,5]thieno[3,2-b][1,2,3]triazolo[4,5-e]indole-2,10-dicarbaldehyde) (**5b**).

5b was synthesized through the same synthetic route as **5a**, and **4b** (0.14g, 0.150 mmol) was used instead of **4a**, affording the orange solid (0.14 g, 93%). ^{1}H NMR (CDCl$_3$, 400 MHz) δ ppm 10.13 (s, 2H), 4.73 (d, J = 7.2 Hz, 2H), 4.61 (d, J = 7.8 Hz, 4H), 3.19 (q, J = 7.7 Hz, 4H), 2.36 (m, 1H), 1.93 (m, 6H), 1.51−0.73 (m, 48H), 0.67−0.50 (m, 12H).

Synthesis of (6,12,13-tris(2-ethylhexyl)-3,9-dioctyl-12,13-dihydro-6H-thieno[2'',3'':4',5']thieno[2',3':4,5]pyrrolo[3,2-g]thieno[2',3':4,5]thieno[3,2-b][1,2,3]triazolo[4,5-e]indole-2,10-dicarbaldehyde) (**5c**).

5c was synthesized through the same synthetic route as **5a**, and **4c** (0.15g, 0.150 mmol) was used instead of **4a**, affording the orange solid (0.14 g, 90%). ^{1}H NMR (CDCl$_3$, 400 MHz) δ ppm 10.13 (s, 2H), 4.73 (d, J = 7.2 Hz, 2H), 4.61 (d, J = 7.8 Hz, 4H), 3.19 (q, J = 7.7 Hz, 4H), 2.38 (m, 1H), 1.93 (m, 6H), 1.52−0.72 (m, 56H), 0.69−0.50 (m, 12H).

Synthesis of (6,12,13-tris(2-ethylhexyl)-3,9-diundecyl-12,13-dihydro-6H-thieno[2'',3'':4',5']thieno[2',3':4,5]pyrrolo[3,2-g]thieno[2',3':4,5]thieno[3,2-b][1,2,3]triazolo[4,5-e]indole-2,10-dicarbaldehyde) (**5d**).

5d was synthesized through the same synthetic route as **5a**, and **4d** (0.16g, 0.150 mmol) was used instead of **4a**, affording the orange solid (0.15 g, 92%). ^{1}H NMR (CDCl$_3$, 400 MHz) δ ppm 10.13 (s, 2H), 4.73 (d, J = 7.2 Hz, 2H), 4.61 (d, J = 7.8 Hz, 4H), 3.19 (q, J = 7.7 Hz, 4H), 2.36 (m, 1H), 1.92 (m, 6H), 1.51−0.72 (m, 68H), 0.69−0.50 (m, 12H).

Synthesis of **YC2**.

Compound **5a** (0.10 g, 0.107 mmol) and 2FIC (0.11 g, 0.481 mmol) were dissolved in CF (25 mL) under argon protection. After adding pyridine (0.8 mL) into the solution, the mixture was stirred at 60 °C overnight. After cooling to room temperature, the reaction mixture was quenched with water and extracted with chloroform. The organic layer was dried over magnesium sulfate and the solvent was removed under reduced pressure. The residue was purified by column chromatography on silica gel by using hexane and dichloromethane as an eluent, yielding dark blue solid (0.13 g, 94%). ^{1}H NMR (CDCl$_3$, 400 MHz) δ ppm 9.13 (s, 2H), 8.55 (dd, J = 10.0, 6.4 Hz, 2H), 7.70 (t, J = 7.5 Hz, 2H), 4.74 (m, 6H), 3.26 (q, J = 7.6 Hz, 4H),

2.34 (m, 1H), 2.02 (m, 2H), 1.56−0.80 (m, 36H), 0.78−0.55 (m, 12H). ^{13}C NMR (CDCl$_3$, 100 MHz) δ ppm 186.14, 159.04, 154.94, 144.59, 137.98, 136.78, 136.68, 135.89, 134.98, 134.50, 133.49, 132.84, 129.83, 119.50, 115.06, 115.02, 114.81, 114.72, 112.06, 68.11, 59.69, 55.47, 40.37, 30.49, 29.65, 28.43, 27.64, 23.99, 23.30, 23.12, 22.95, 22.77, 15.26, 24.05, 13.71, 10.54, 10.24. HRMS (ESI) *m/z* 1294.4285 (C$_{72}$H$_{67}$F$_4$N$_9$O$_2$S$_4$ calcd. for *m/z* 1294.4270)

Synthesis of **YC6**.

YC6 was synthesized through the same synthetic route as **YC2**, and **5b** (0.11 g, 0.107 mmol) was used instead of **5a**, yielding dark blue solid (0.14 g, 91%). ^{1}H NMR (CDCl$_3$, 400 MHz) δ ppm 9.14 (s, 2H), 8.55 (dd, *J* = 10.0, 6.4 Hz, 2H), 7.70 (t, *J* = 7.5 Hz, 2H), 4.73 (m, 6H), 3.23 (t, *J* = 7.9 Hz, 4H), 2.35 (m, 1H), 2.01 (m, 2H), 1.88 (m, 4H), 1.51−0.81 (m, 48H), 0.73−0.54 (m, 12H). ^{13}C NMR (CDCl$_3$, 100 MHz) δ ppm 186.17, 159.11, 154.00, 145.02, 137.97, 136.60, 135.91, 135.88, 135.27, 135.24, 133.47, 133.20, 129.76, 119.48, 115.15, 115.03, 114.80, 114.76, 112.02, 68.14, 59.75, 55.46, 40.37, 31.66, 31.29, 30.46, 29.89, 29.63, 29.54, 28.40, 27.61, 23.98, 23.32, 22.96, 22.76, 22.57, 14.10, 14.05, 13.70, 10.55, 10.26. HRMS (ESI) *m/z* 1406.5530 (C$_{80}$H$_{83}$F$_4$N$_9$O$_2$S$_4$ calcd. for *m/z* 1406.5522)

Synthesis of **YC8**.

YC8 was synthesized through the same synthetic route as **YC2**, and **5c** (0.11 g, 0.107 mmol) was used instead of **5a**, yielding dark blue solid (0.15 g, 93%). ^{1}H NMR (CDCl$_3$, 400 MHz) δ ppm 9.14 (s, 2H), 8.55 (dd, *J* = 10.0, 6.5 Hz, 2H), 7.70 (t, *J* = 7.5 Hz, 2H), 4.73 (m, 6H), 3.23 (t, *J* = 7.9 Hz, 4H), 2.36 (m, 1H), 2.01 (m, 2H), 1.88 (m, 4H), 1.55−0.81 (m, 56H), 0.76−0.57 (m, 12H). ^{13}C NMR (CDCl$_3$, 100 MHz) δ ppm 186.18, 159.05, 154.01, 148.45, 145.03, 137.97, 136.60, 135.91, 135.24, 134.48, 133.46, 133.21, 129.81, 119.47, 115.15, 114.81, 114.76, 112.03, 68.11, 59.76, 55.46, 40.36, 31.88, 31.31, 30.46, 29.87, 29.63, 29.45, 29.20, 28.41, 27.61, 23.98, 23.32, 22.96, 22.76, 22.68, 14.14, 14.05, 13.70, 10.54, 10.25. HRMS (ESI) *m/z* 1462.6218 (C$_{84}$H$_{91}$F$_4$N$_9$O$_2$S$_4$ calcd. for *m/z* 1462.6148)

Synthesis of **YC11**.

YC11 was synthesized through the same synthetic route as **YC2**, and **5d** (0.12 g, 0.107 mmol) was used instead of **5a**, yielding dark blue solid (0.15 g, 91%). ^{1}H NMR (CDCl$_3$, 400 MHz) δ ppm 9.14 (s, 2H), 8.55 (dd, *J* = 10.0, 6.5 Hz, 2H), 7.70 (t, *J* = 7.5 Hz, 2H), 4.73 (m, 6H), 3.23 (t, *J* = 7.9 Hz, 4H), 2.36 (m, 1H), 2.01 (m, 2H), 1.87 (m, 4H), 1.55−0.81 (m, 68H), 0.77−0.55 (m, 12H). ^{13}C NMR (CDCl$_3$, 100 MHz) δ ppm 186.19, 159.00, 154.01, 145.02, 137.97, 136.59, 135.91, 135.25, 134.52, 134.37, 133.46, 133.21, 129.76, 119.47, 115.15, 115.01, 114.79, 114.76, 112.03, 68.14, 59.73, 55.44, 40.36, 31.93, 31.33, 30.46, 29.89, 29.67, 29.64, 29.55,

29.52, 29.36, 28.41, 27.61, 23.97, 23.32, 22.96, 22.77, 22.71, 14.14, 14.05, 13.70, 10.54, 10.25. HRMS (ESI) m/z 1546.7009 ($C_{90}H_{103}F_4N_9O_2S_4$ calcd. for m/z 1546.7087)

OSCs fabrication and characterization

The OSCs were fabricated with a configuration of indium tin oxide (ITO)/ poly(3,4-ethylenedioxythiophene):poly(styrene sulfonate) (PEDOT:PSS)/active layer/aliphatic amine-functionalized perylene-diimide (PDINN)/Ag. PEDOT:PSS (Bayer Baytron4083) was spin-coated at 4000 rpm onto the ITO substrate, followed by annealing at 135 °C for 20 min in air. The PM6:YCx (D:A = 1:1.4 wt%), were dissolved with 14.5 mg mL^{-1} total concentration in CF:CB ($v:v$ = 100:0, 90:10, 80:20, 70:30 vol%) solutions, respectively. After stirring the solution for 2 hours, 0.5 vol% of CN additive was added, followed by stirring for an additional 30 min. Subsequently, the solutions were blade coating onto the PEDOT:PSS layer with 400 μm blade gap for 20 mm s^{-1} blade speed. The thicknesses of the fabricated films were around 120 nm. The films were treated with thermal annealing at 100 °C for 10 min. Then methanol solution of PDINN (0.8 mg mL^{-1}) was then deposited onto the active layer with a spin rate of 3000 rpm for 30 s. Finally, 100 nm silver was vacuum deposited under vacuum (< 3.0×10^{-6} Pa). The active area of each sample was 4.2 mm^2 and 1.05 cm^2. The current density versus voltage (J–V) characteristics were recorded using a Keithley 2400 source under illumination of an AM 1.5G solar simulator with an intensity of 100 mW cm^{-2} calculated by Oriel 91150V-CBL reference solar cell. The J–V curves were obtained without the use of an optical mask. The thickness of the active layers was measured using a stylus profilometer (P6, KLA Tencor).

The hole and electron mobilities of neat and blend films were measured via using the SCLC method. Device structures are ITO/PEDOT:PSS/active layer/Au for hole-only devices and ITO/ZnO/active layer/PDINN/Ag for electron-only devices, respectively. The area of the single carrier devices is 4.2 mm^2. The SCLC mobilities were calculated using the Mott–Gurney equation, $J = 9\varepsilon_r\varepsilon_0\mu V^2/8L^3$, where ε_r is the relative dielectric constant of the organic semiconductor, ε_0 is the permittivity of empty space, m is the mobility of zero-field, L is the thickness of the active layer, and $V = V_{applied} - V_{built-in} - V_{series-resistance}$ (the V_{bi} values are estimated as 0.2 V and 0 V for the hole-only and the electron-only devices, respectively),[3] where $V_{applied}$ is the voltage applied, and $V_{built-in}$ is the built-in voltage from the relative work function difference between the two electrodes. $V_{series-resistance}$ is the voltage caused by the series and

contact resistance potential drop ($V_{\text{series-resistance}} = J \times R_{\text{series-resistance}}$). For convenience, the voltage drops caused by this resistance ($R_{\text{series-resistance}}$) was ignored.

The EQE measurements were conducted using Model QE-R3011 (Enlitech) in ambient air. EQE$_{\text{EL}}$ measurements were performed by applying external voltage/current sources through the devices (ELCT-3010, Enlitech). All of the devices were prepared for EQE$_{\text{EL}}$ measurements according to the optimal device fabrication conditions. EQE$_{\text{EL}}$ measurements were carried out from 0.7 to 2 V).

In situ PL and in situ UV–Vis spectroscopy measurement

In situ PL spectra were measured using ELCT-3010 PL mode (Enlitech). The integration time of in situ PL was 5 ms with automatically recoded spectra every 10 ms. In situ UV-Vis spectra were measured using UV-Vis microspectrometer (CRAIC). Full range scan time of in situ UV-Vis measurement is 7 ms with 100 ms interval for every single scan. In situ PL and in situ UV-Vis spectroscopy were used to track the film formation process of the blade-coated blend solutions. The conditions for the blade coating (i.e., blade gap, blade speed, substrate temperature, and solution concentration) were the same as the conditions for fabricating the OSC films.
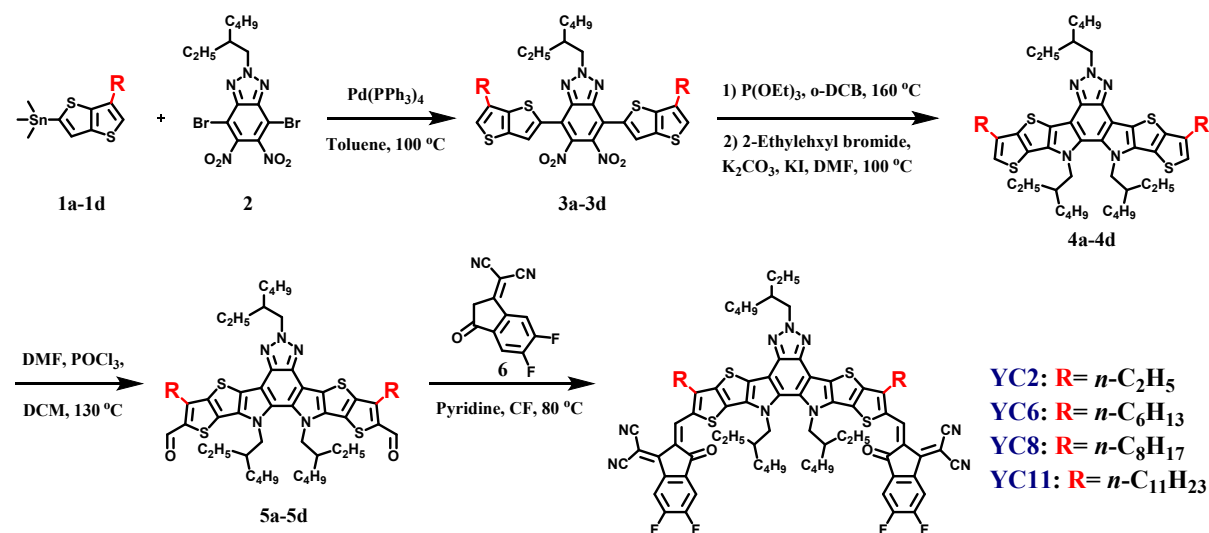
Fig. S1 Synthetic routes of the NFAs.
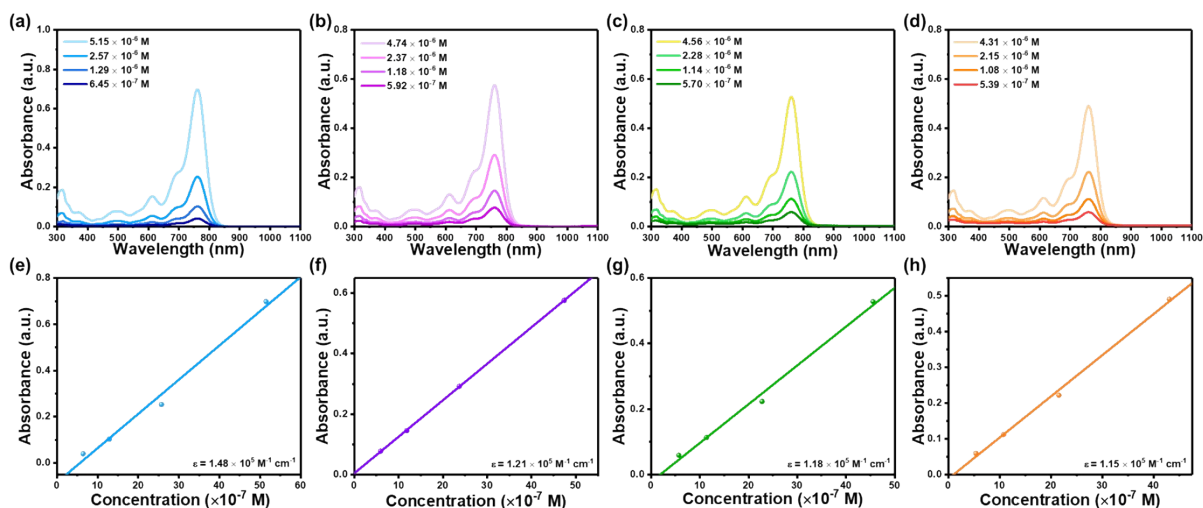
Fig. S2 UV-Vis absorption spectra on different concentrations of the NFA in CF solutions and calibration plots of the absorbance of the NFA versus the measured concentration for (a, e) YC2, (b, f) YC6 (c, g) YC8, and (d, h) YC11.
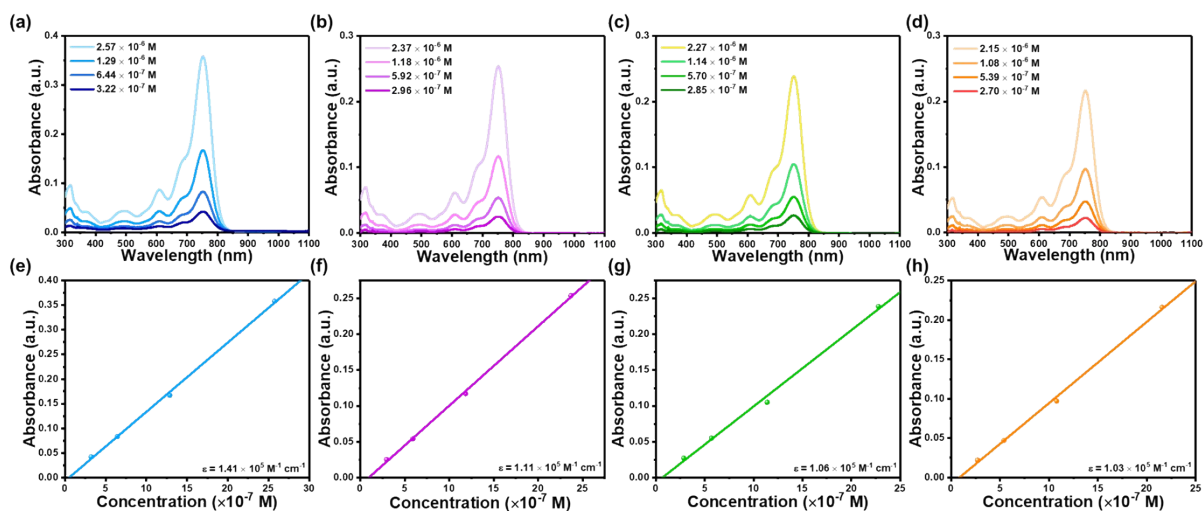
Fig. S3 UV-Vis absorption spectra on different concentrations of the NFA in CB solutions and calibration plots of the absorbance of the NFA versus the measured concentration for (a, e) YC2, (b, f) YC6 (c, g) YC8, and (d, h) YC11.
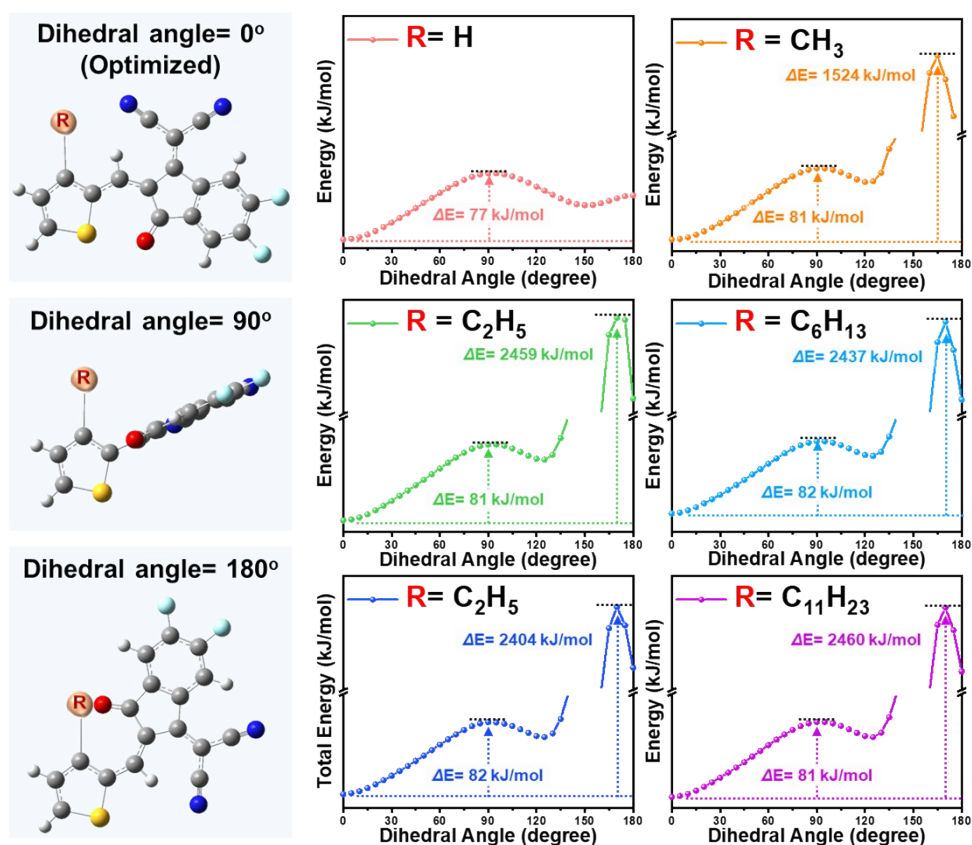
Fig. S4 Energy−torsion angle curve between the different outer side-chains-containing thiophene and 2FIC units.
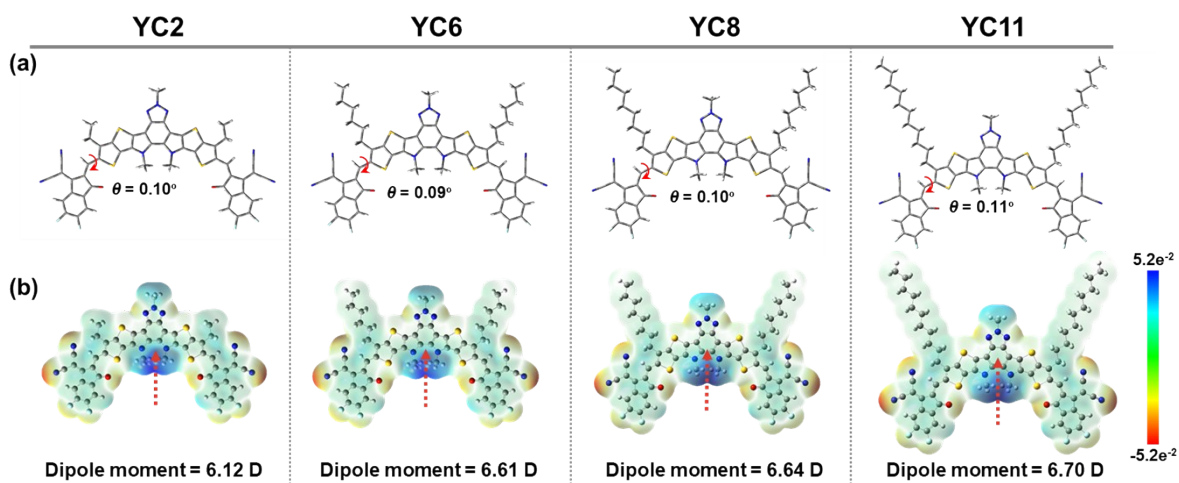
Fig. S5 (a) Optimized geometry of NFAs. (b) Electrostatic potential and dipole moment of NFAs.
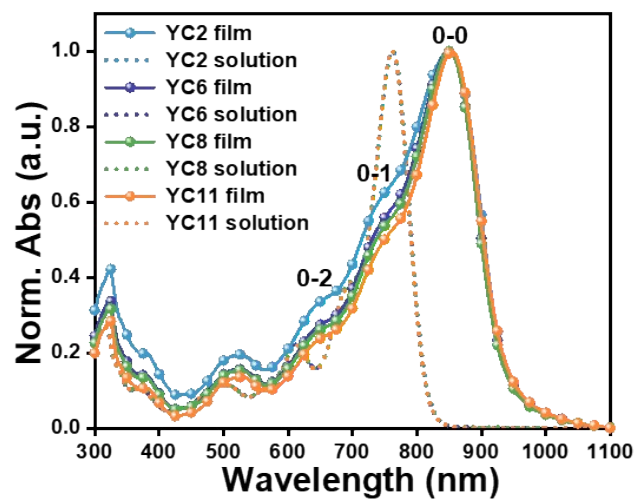
Fig. S6 Normalized absorption spectra of NFAs in CF solution and thin films.
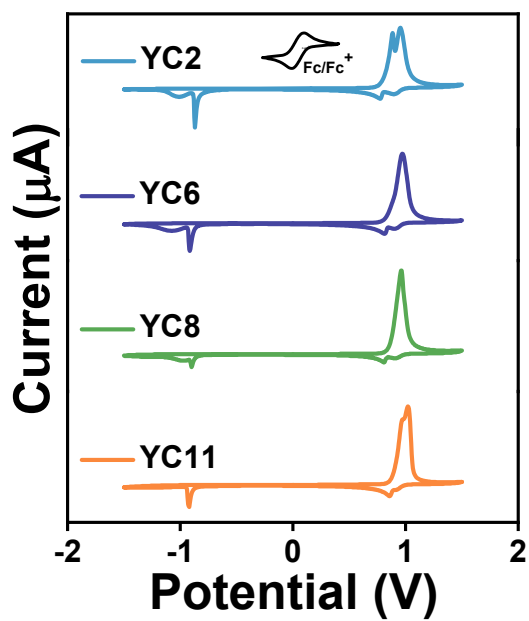
Fig. S7 CV curve of NFAs.
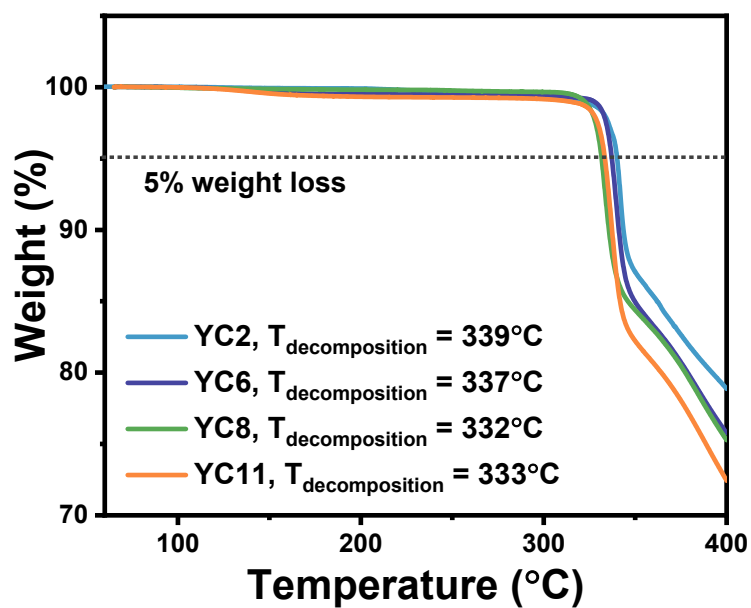
Fig. S8 TGA heating curves of NFAs.
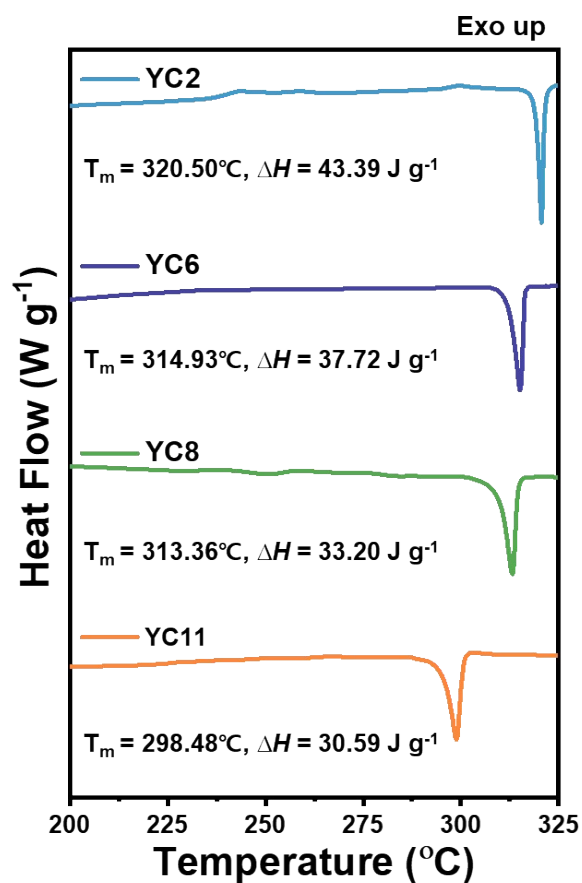
Fig. S9 DSC heating curves of NFAs.
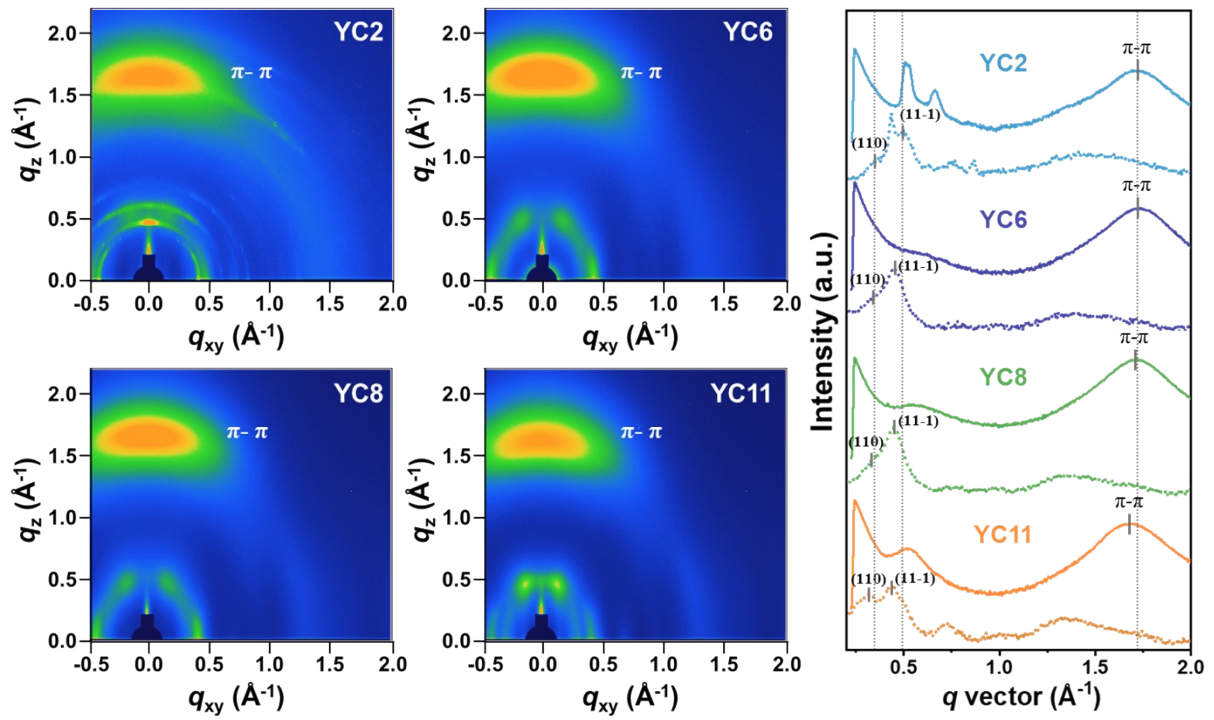
Fig. S10 GIWAXS pattern of NFA neat films and their corresponding line-cut profiles.

Table S1. Detailed GIWAXS parameters of the NFA neat films.

| Neat film | Out-of-Plane | | | In-Plane | | | | | |
| | π-π stacking peak | | | (110) peak | | | (11-1) peak | | |
	q (Å^{-1})	d-spacing (Å)	Coherence length (Å)	q (Å^{-1})	d-spacing (Å)	Coherence length (Å)	q (Å^{-1})	d-spacing (Å)	Coherence length (Å)
YC2	1.72	3.66	20.32	0.39	16.11	55.47	0.48	13.09	80.86
YC6	1.72	3.66	19.03	0.38	16.70	54.40	0.45	13.89	78.60
YC8	1.71	3.67	19.00	0.36	17.37	53.87	0.45	13.97	75.17
YC11	1.69	3.72	17.95	0.31	20.25	53.37	0.44	14.30	65.56
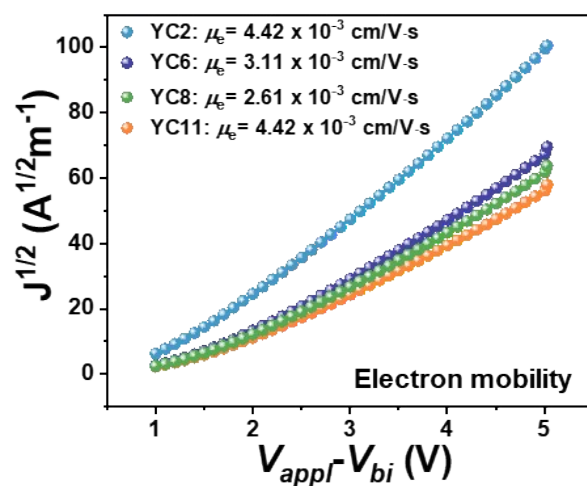
Fig. S11 SCLC plot and electron mobility of NFA neat films.
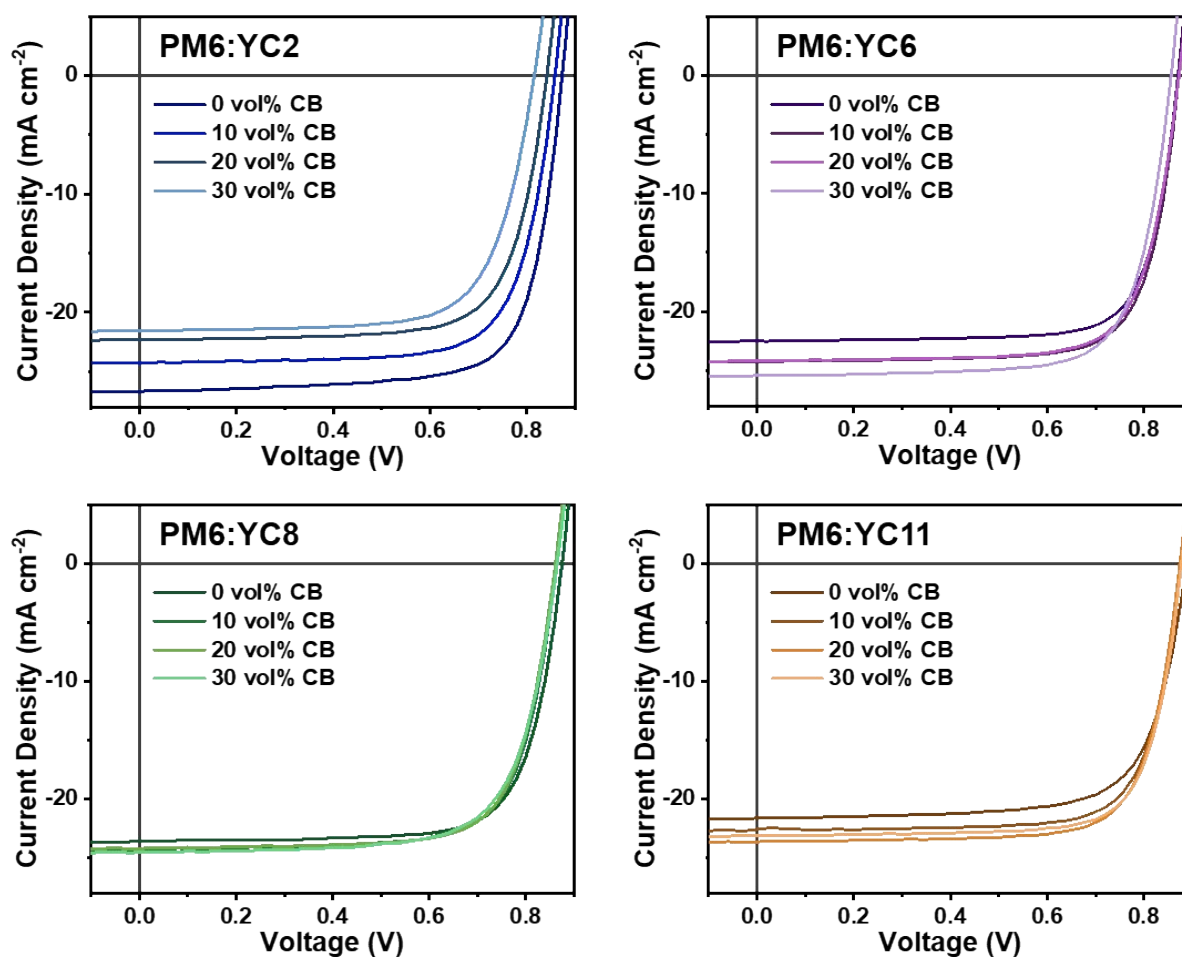
Fig. S12 *J–V* characteristics of OSCs.
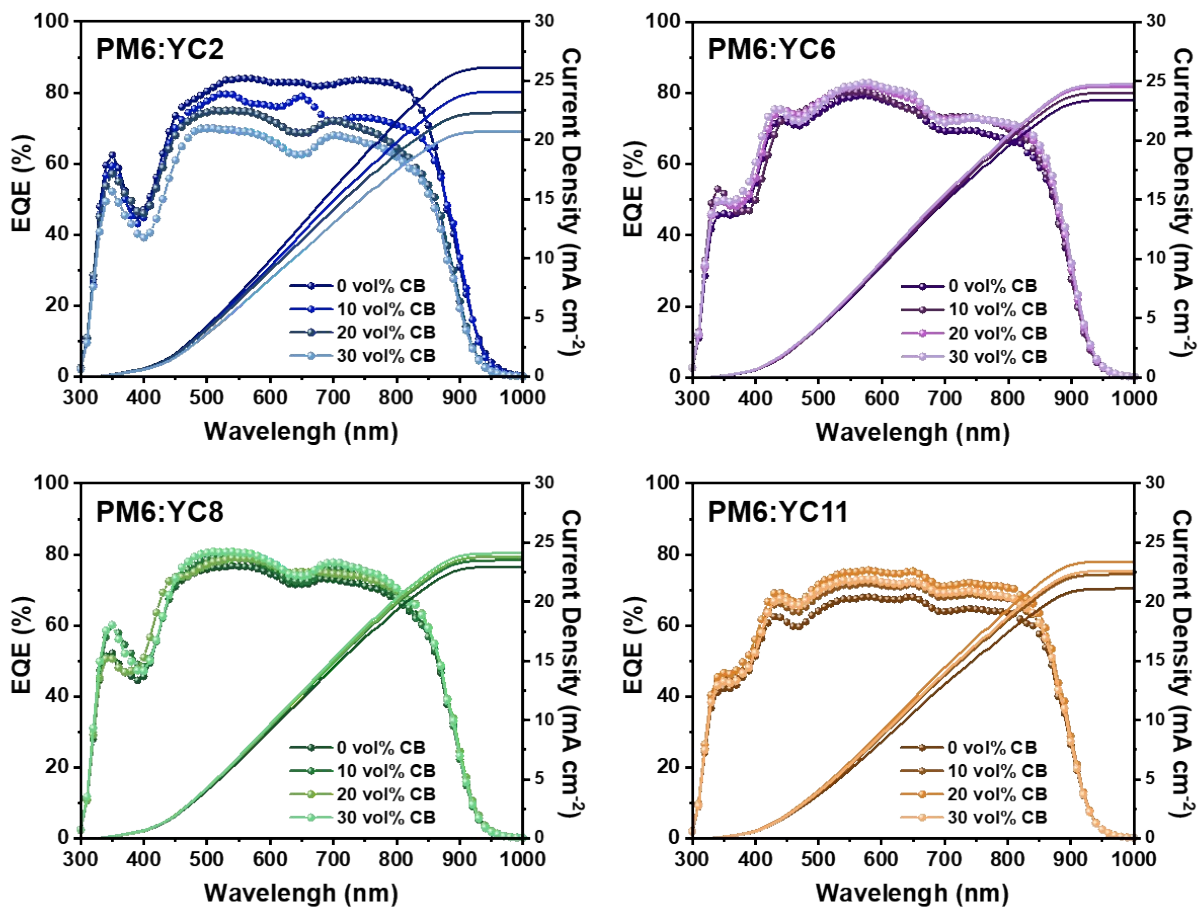
Fig. S13 EQE spectra and integrated current density of OSCs.
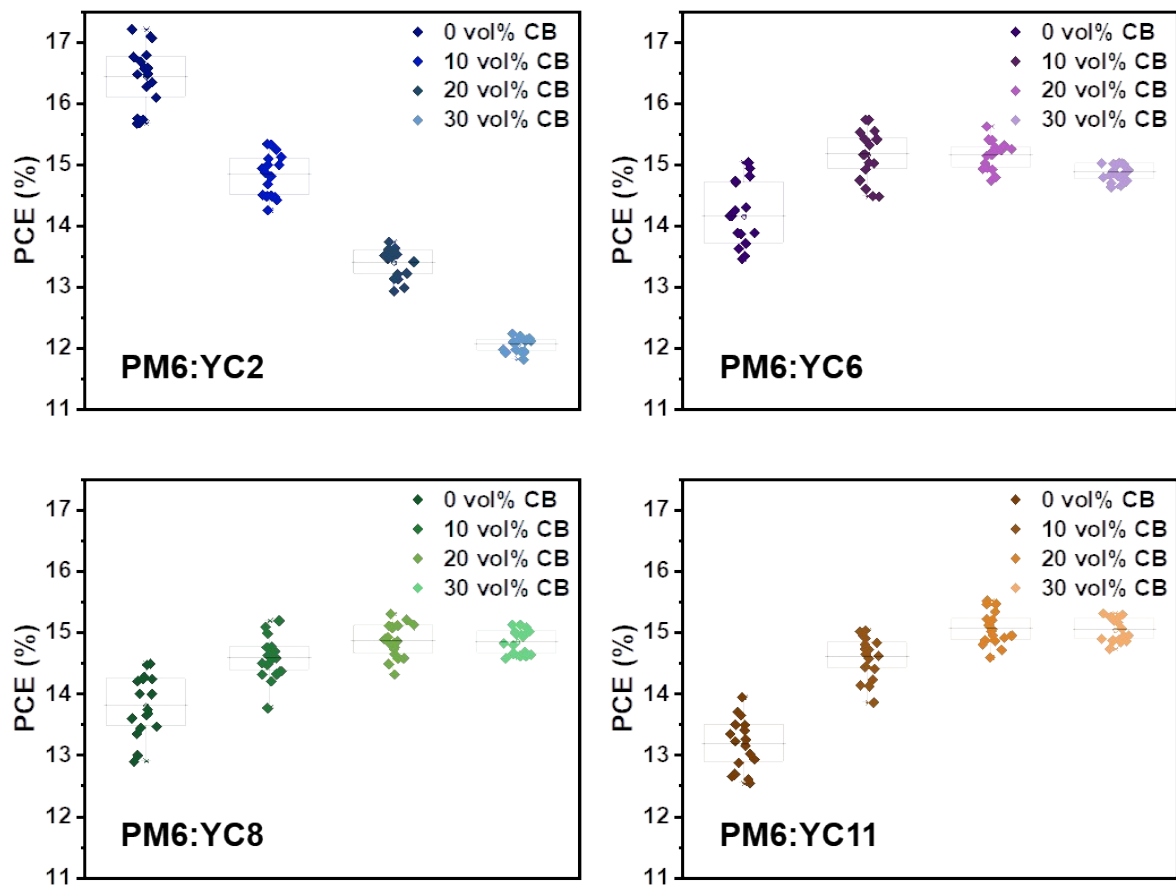
Fig. S14 Statistical distributions of PCEs from 17 OSCs.
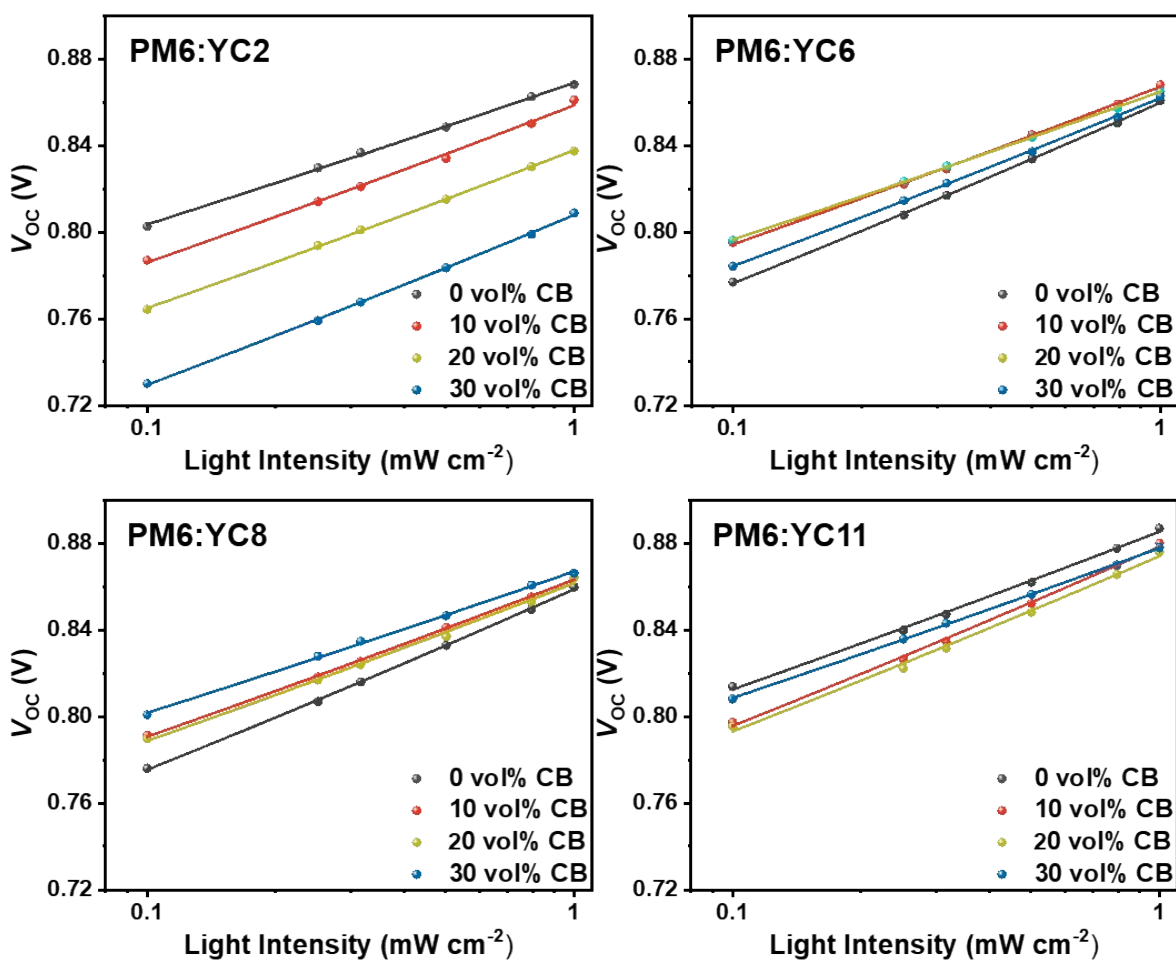
Fig. S15 Light intensity-dependent plots of V_{OC} versus I for the OSCs.
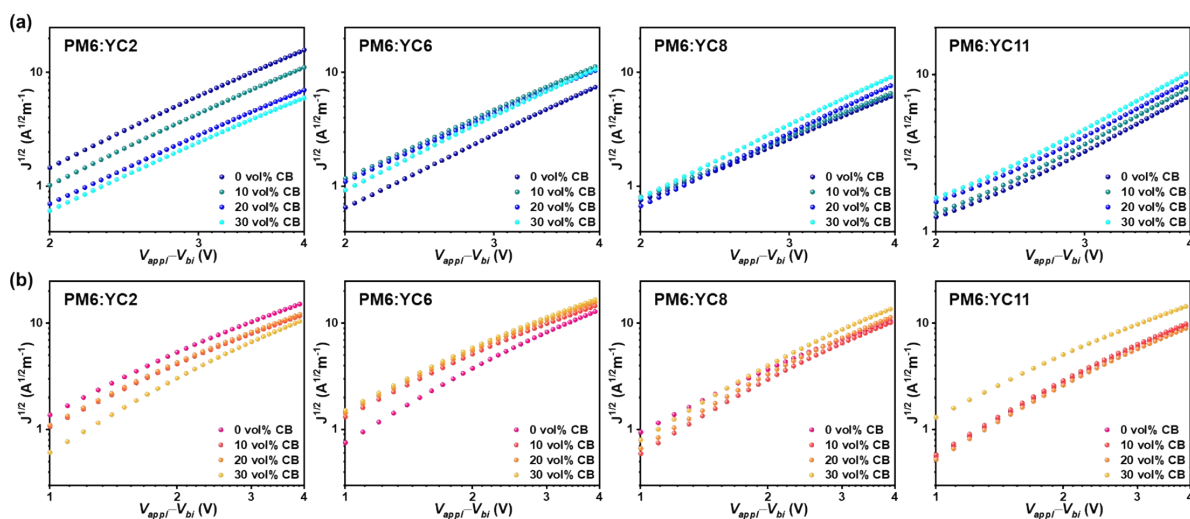
Fig. S16 SCLC plots of (a) electron- and (b) hole-only devices for the blade-coated blend films.

Table S2. Summary of recombination parameters and mobilities of OSCs.

NFA/CB vol% in cosolvent	S (kT/q)	μ_h ($cm^2 V^{-1} s^{-1}$)	μ_e ($cm^2 V^{-1} s^{-1}$)	μ_h/μ_e
YC2/0 vol%	1.31	6.4×10^{-4}	6.1×10^{-4}	1.05
YC2/10 vol%	1.48	4.3×10^{-4}	3.1×10^{-4}	1.39
YC2/20 vol%	1.52	4.8×10^{-4}	2.1×10^{-4}	2.29
YC2/30 vol%	1.70	3.9×10^{-4}	1.4×10^{-4}	2.79
YC6/0 vol%	1.30	6.1×10^{-4}	4.5×10^{-4}	1.36
YC6/10 vol%	1.46	6.3×10^{-4}	5.7×10^{-4}	1.11
YC6/20 vol%	1.47	6.4×10^{-4}	5.6×10^{-4}	1.14
YC6/30 vol%	1.47	6.7×10^{-4}	5.8×10^{-4}	1.16
YC8/0 vol%	1.31	3.7×10^{-4}	3.3×10^{-4}	1.12
YC8/10 vol%	1.42	3.8×10^{-4}	3.4×10^{-4}	1.11
YC8/20 vol%	1.45	4.6×10^{-4}	4.4×10^{-4}	1.05
YC8/30 vol%	1.45	5.5×10^{-4}	5.2×10^{-4}	1.06
YC11/0 vol%	1.44	3.0×10^{-4}	3.4×10^{-4}	0.88
YC11/10 vol%	1.45	3.2×10^{-4}	3.5×10^{-4}	0.91
YC11/20 vol%	1.42	4.2×10^{-4}	4.3×10^{-4}	0.98
YC11/30 vol%	1.44	5.0×10^{-4}	4.7×10^{-4}	1.06
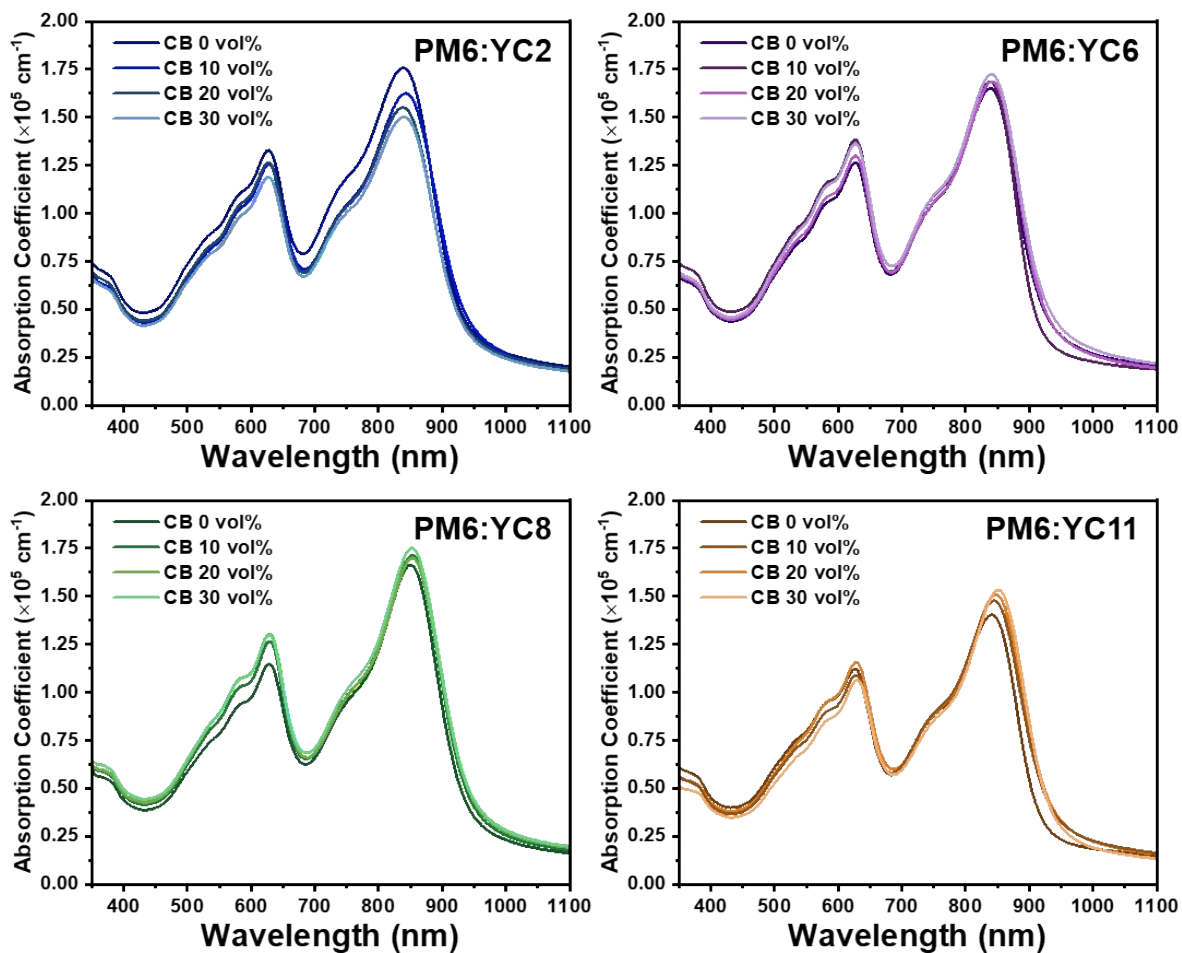
Fig. S17 Absorption coefficient of blend films.
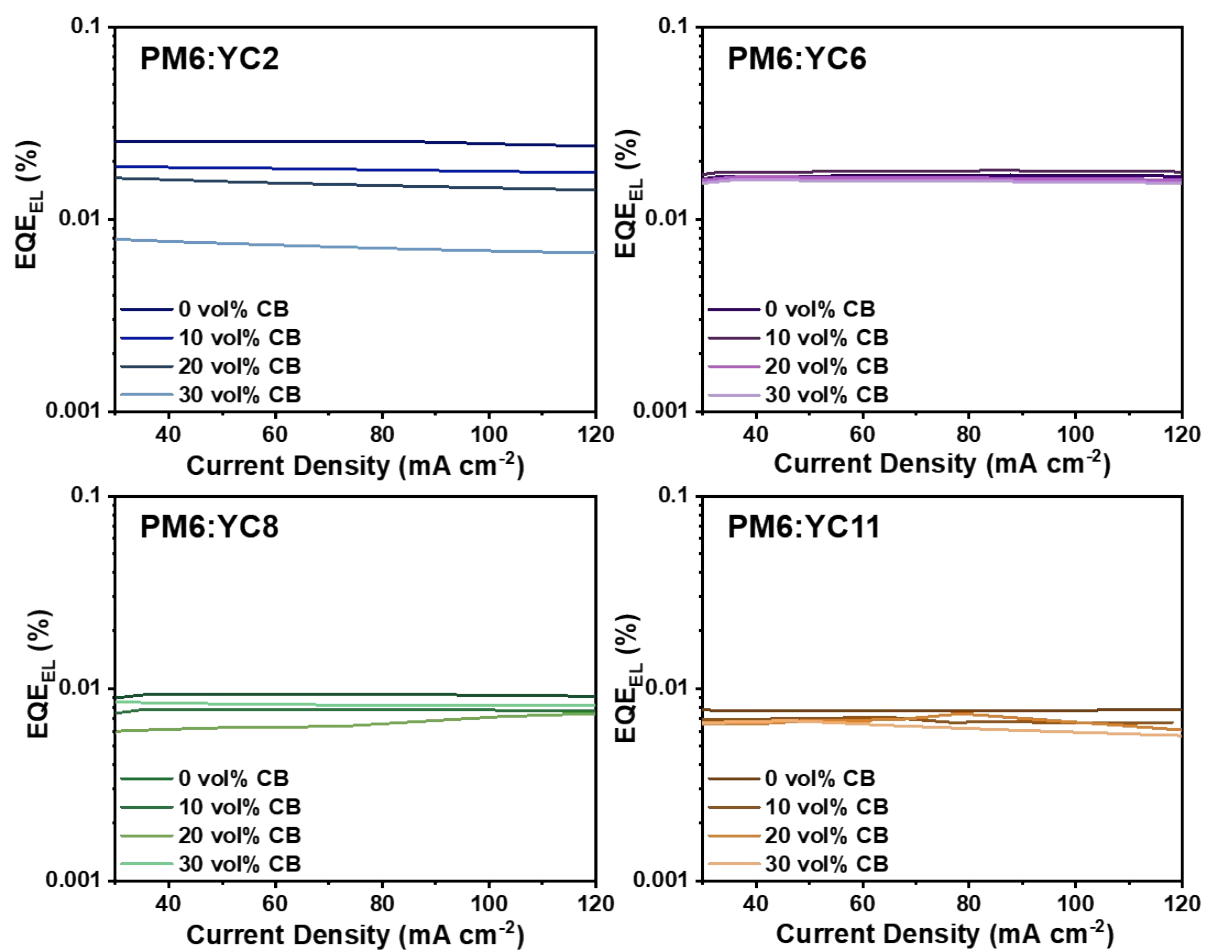
Fig. S18 EQE$_{EL}$ plot of OSCs

Table S3. Summary of E_g and E_{loss} parameters of OSCs

NFA/CB vol% in cosolvent	E_g (eV)	E_{loss} (eV)	ΔE_1 (eV)	ΔE_2 (eV)	EQE_{EL} (%)	ΔE_3 (eV)
YC2/0 vol%	1.384	0.503	0.26	0.029	0.02540	0.214
YC2/10 vol%	1.383	0.526	0.263	0.041	0.01864	0.222
YC2/20 vol%	1.383	0.547	0.261	0.061	0.01660	0.225
YC2/30 vol%	1.383	0.572	0.262	0.067	0.00827	0.243
YC6/0 vol%	1.390	0.526	0.260	0.041	0.01662	0.225
YC6/10 vol%	1.390	0.527	0.260	0.044	0.01793	0.223
YC6/20 vol%	1.390	0.526	0.260	0.041	0.01660	0.225
YC6/30 vol%	1.390	0.528	0.260	0.042	0.01597	0.226
YC8/0 vol%	1.403	0.543	0.260	0.041	0.00929	0.240
YC8/10 vol%	1.405	0.545	0.260	0.039	0.00766	0.245
YC8/20 vol%	1.405	0.542	0.260	0.037	0.00766	0.245
YC8/30 vol%	1.404	0.543	0.260	0.039	0.00827	0.243
YC11/0 vol%	1.410	0.531	0.258	0.028	0.00763	0.245
YC11/10 vol%	1.411	0.537	0.257	0.033	0.00709	0.247
YC11/20 vol%	1.411	0.538	0.259	0.033	0.00737	0.246
YC11/30 vol%	1.410	0.537	0.258	0.031	0.00682	0.248
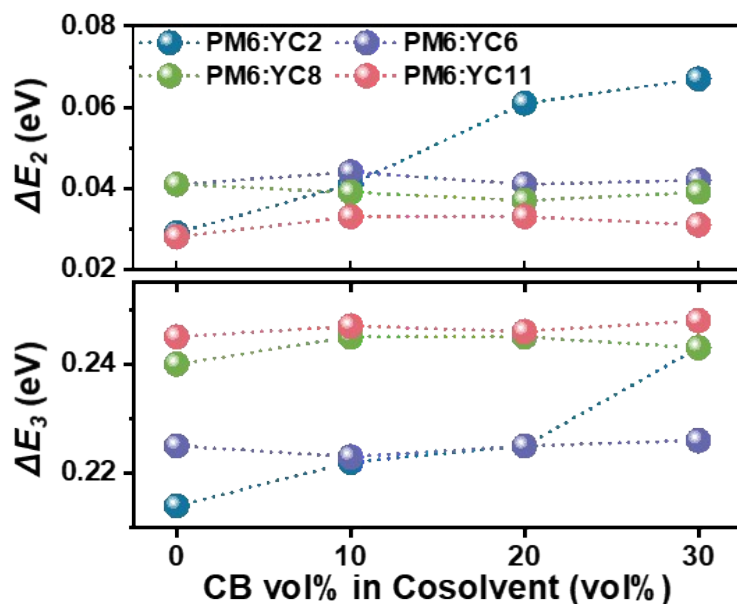
Fig. S19 Comparison of ΔE_2 and ΔE_3 of OSCs fabricated under different cosolvent conditions.
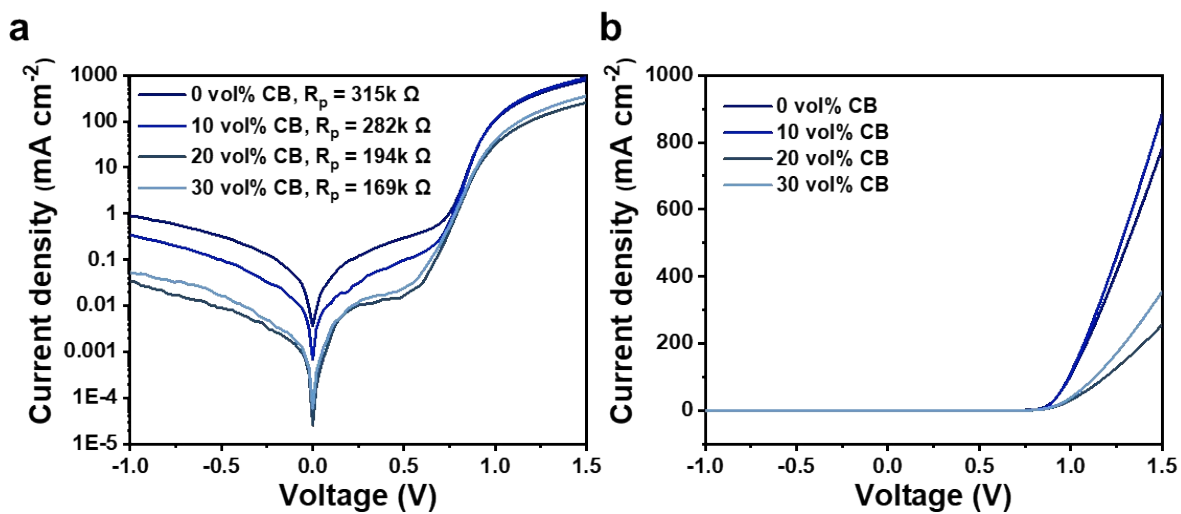
Fig. S20 Dark current measurement of YC2-based OSCs and calculated parallel resistance of the OSCs. (a) log-scale Dark *J–V* plot and (b) linear-scale dark *J–V* plot.
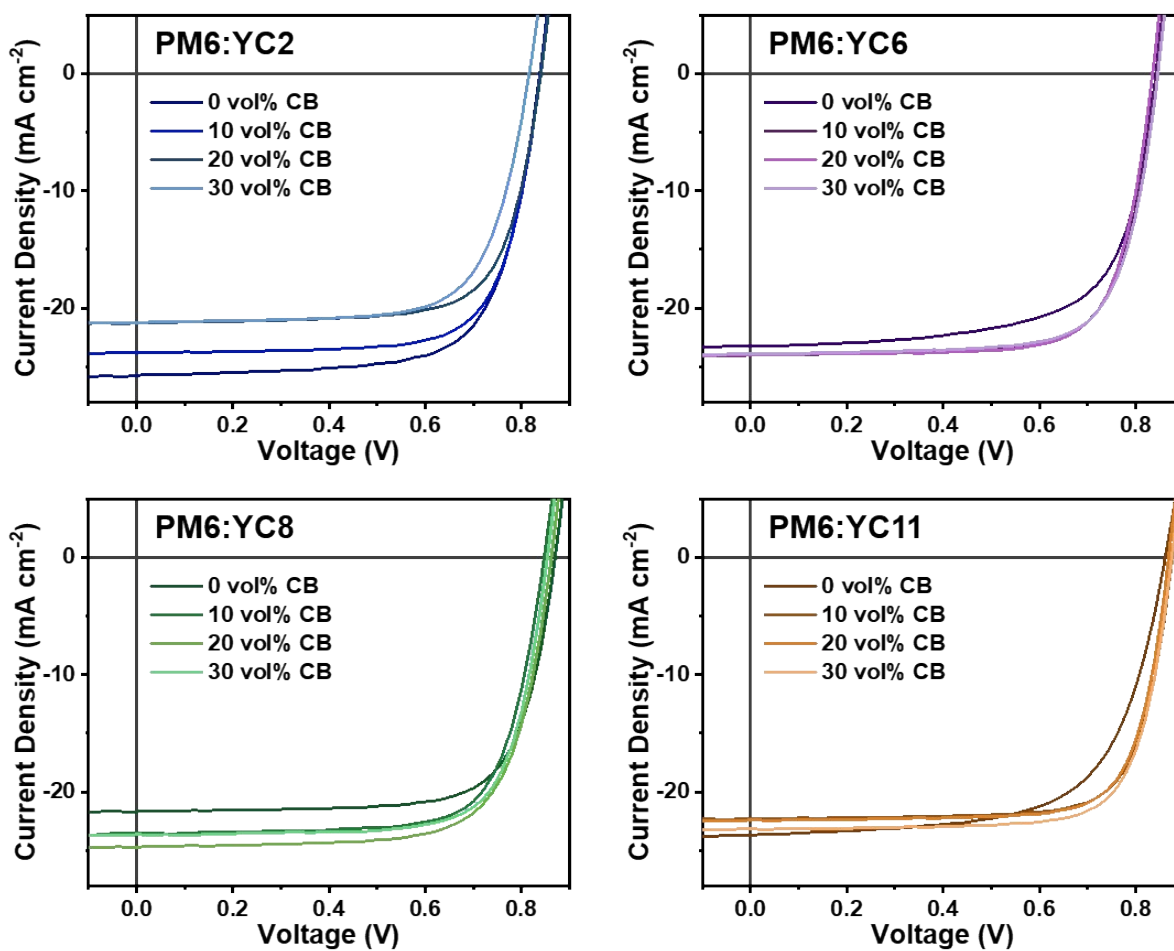
Fig. S21 *J-V* characteristics of large-area (1.05 cm^2) OSCs.
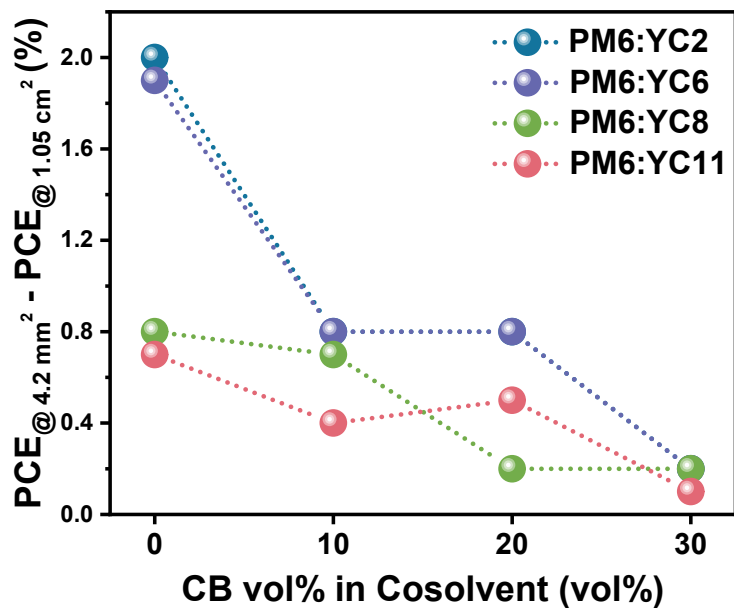
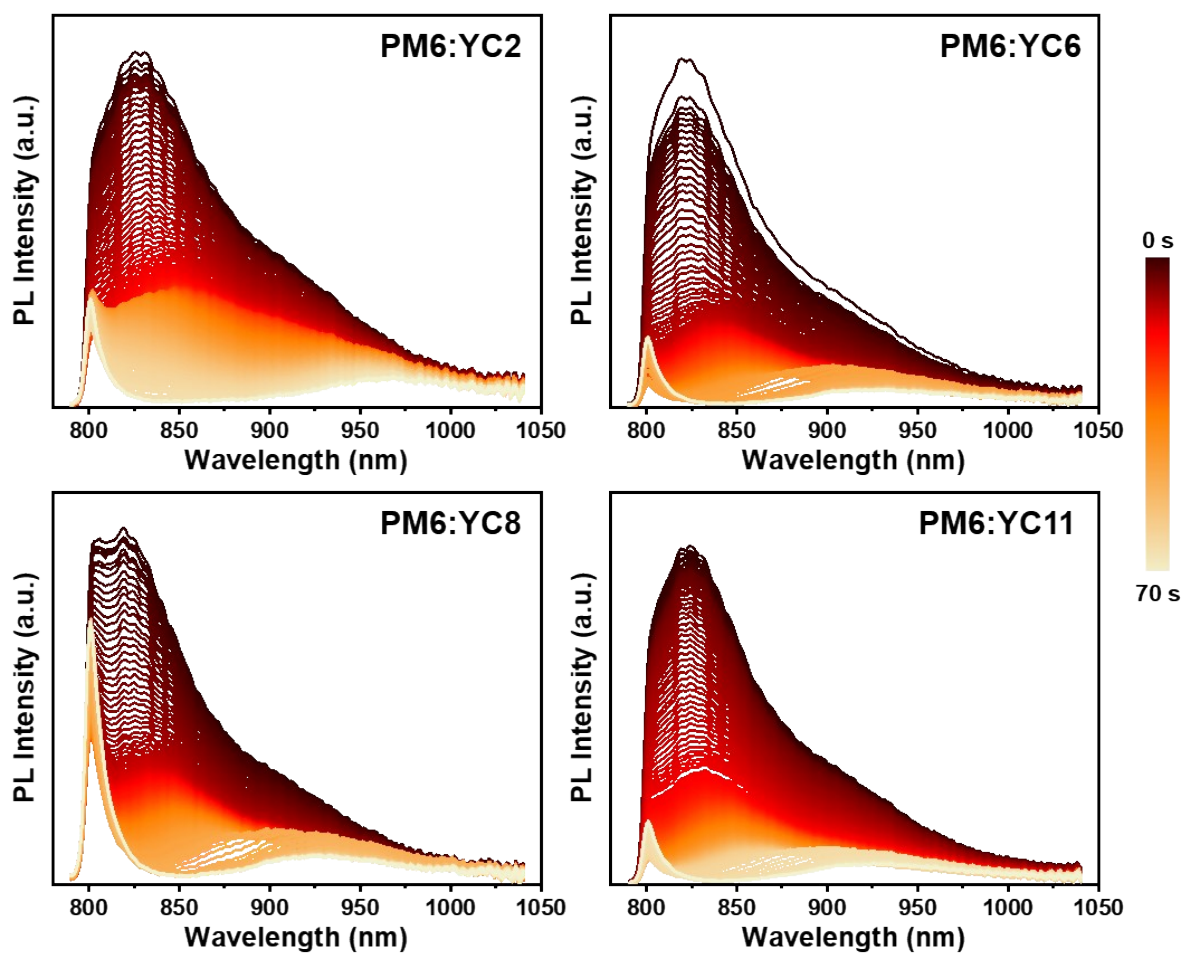**Fig. S22** PCE difference between small (4.2 mm^2) and large-area (1.05 cm^2) OSCs.
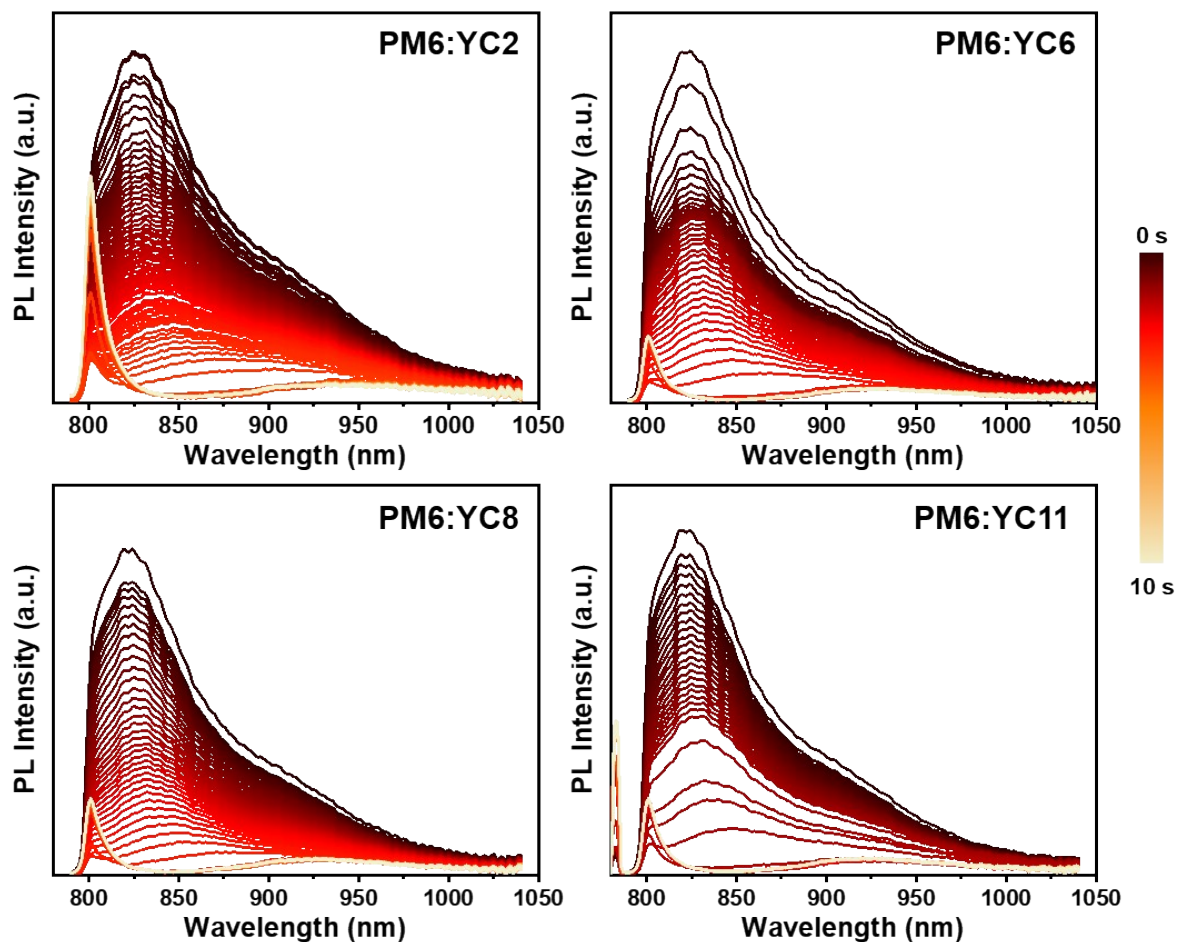
Fig. S23 In situ PL spectra of blade-coated blends under 0 vol% CB cosolvent condition excited at @720nm.
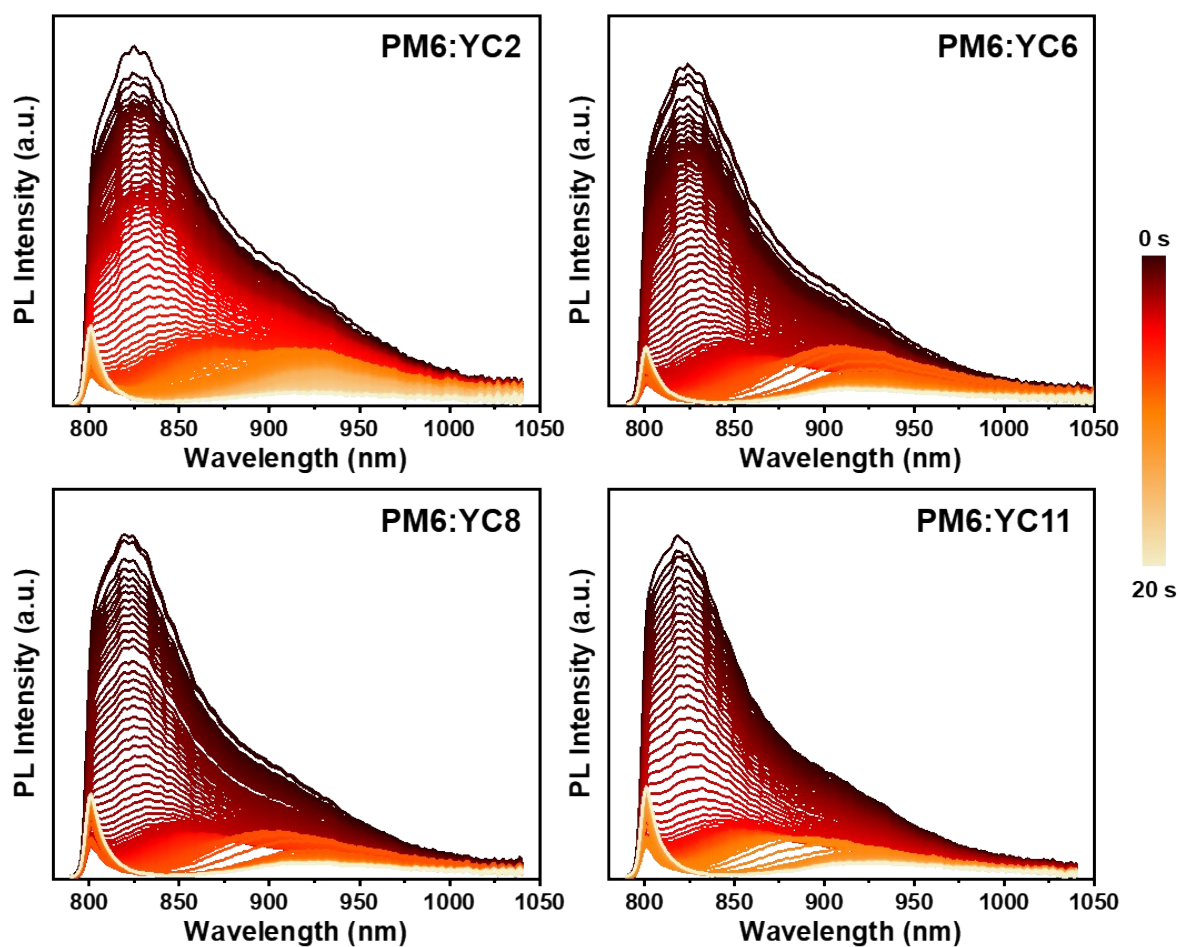
Fig. S24 In situ PL spectra of blade-coated blends under 10 vol% CB cosolvent condition excited at @720nm.
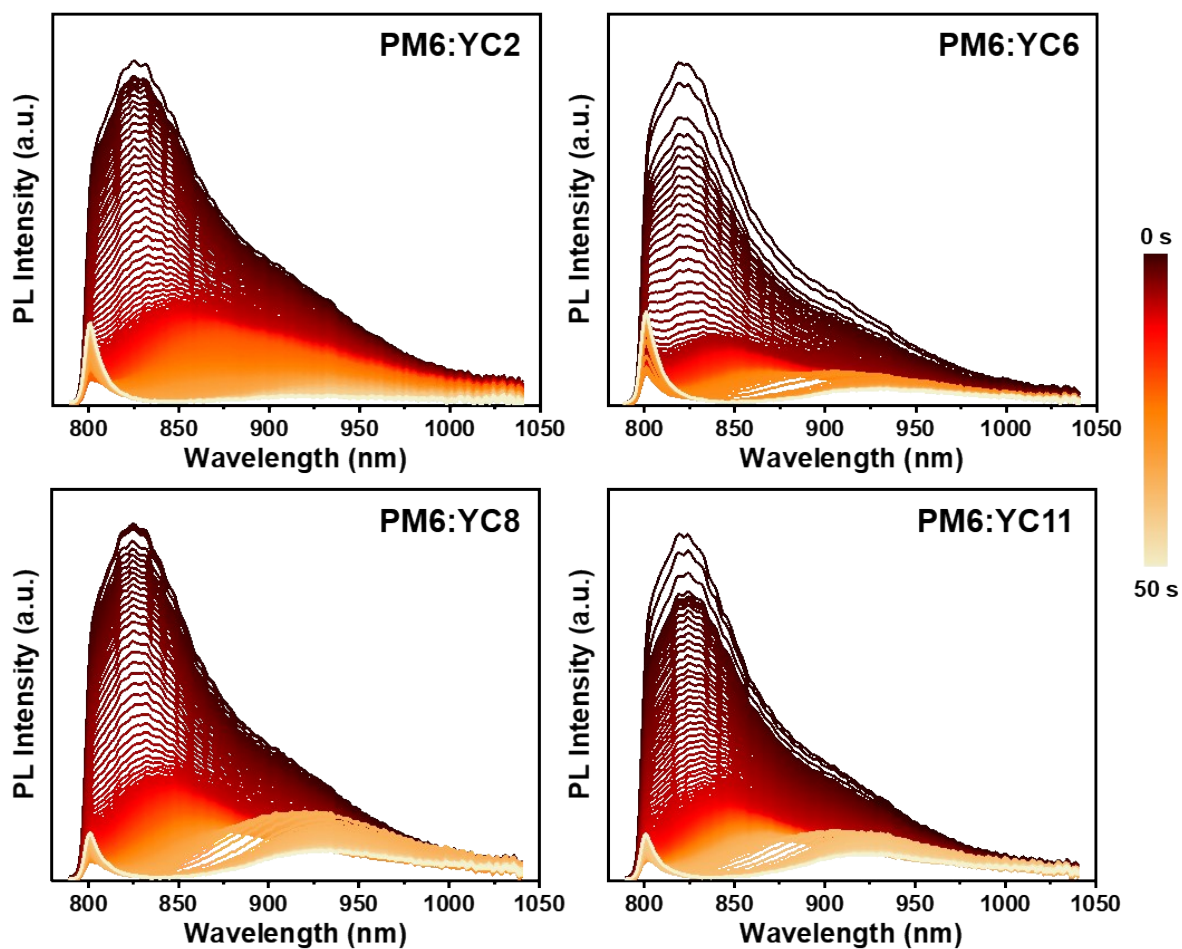
Fig. S25 In situ PL spectra of blade-coated blends under 20 vol% CB cosolvent condition excited at @720nm.

Fig. S26 In situ PL spectra of blade-coated blends under 30 vol% CB cosolvent condition excited at @720nm.
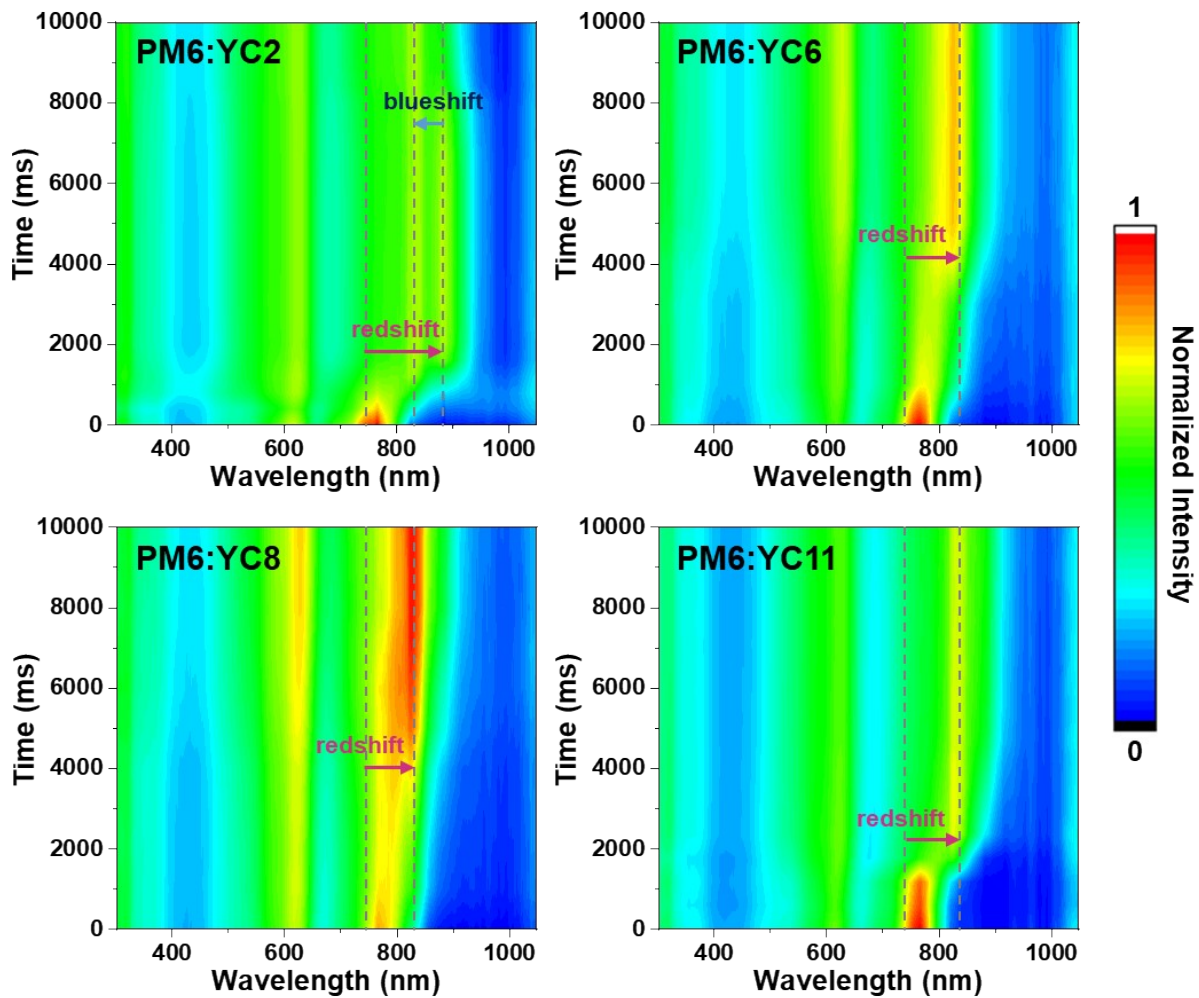
Fig. S27 In situ UV-Vis spectra of blade-coated blends under 0 vol% CB cosolvent condition.
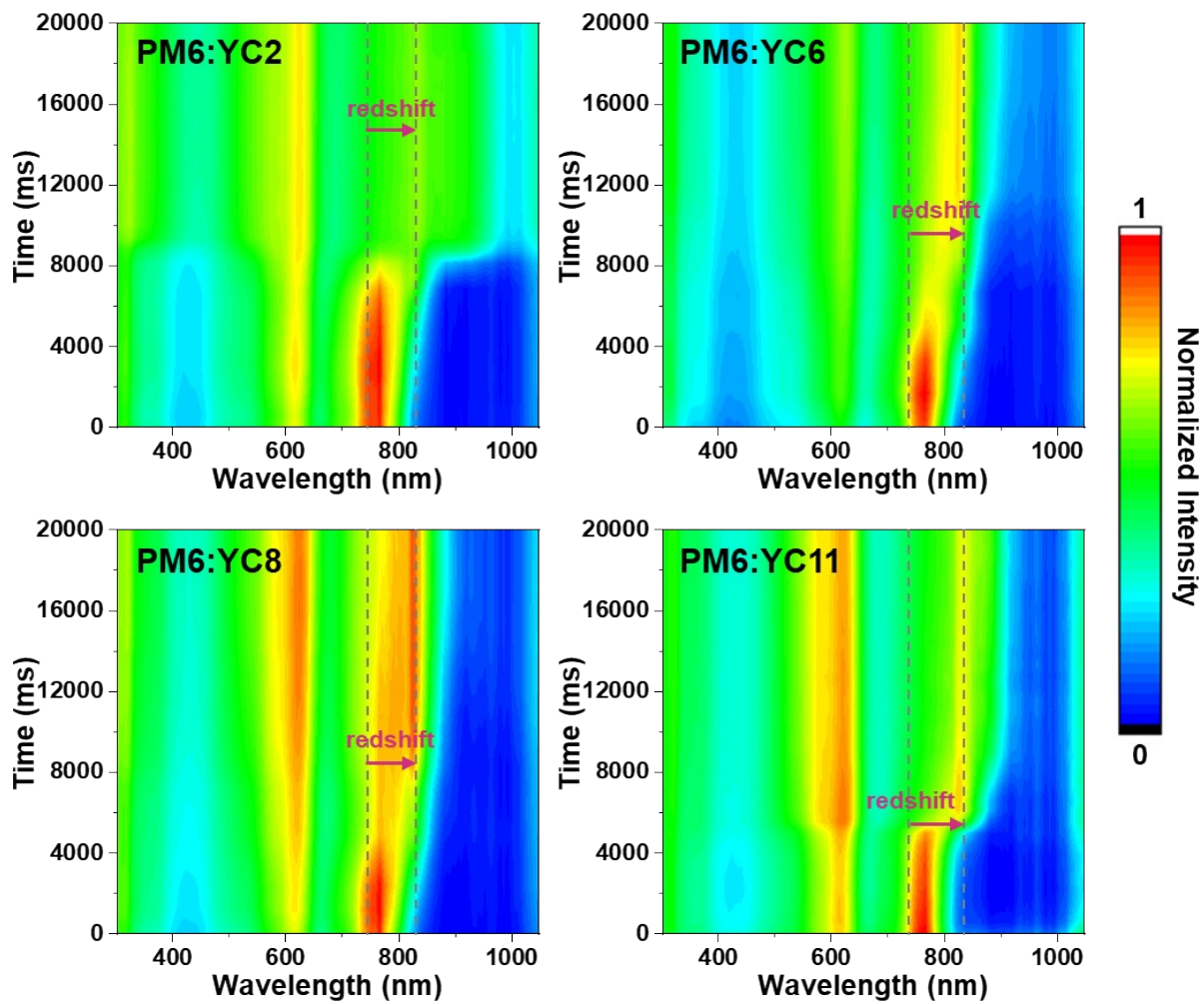
Fig. S28 In situ UV-Vis spectra of blade-coated blends under 10 vol% CB cosolvent condition.
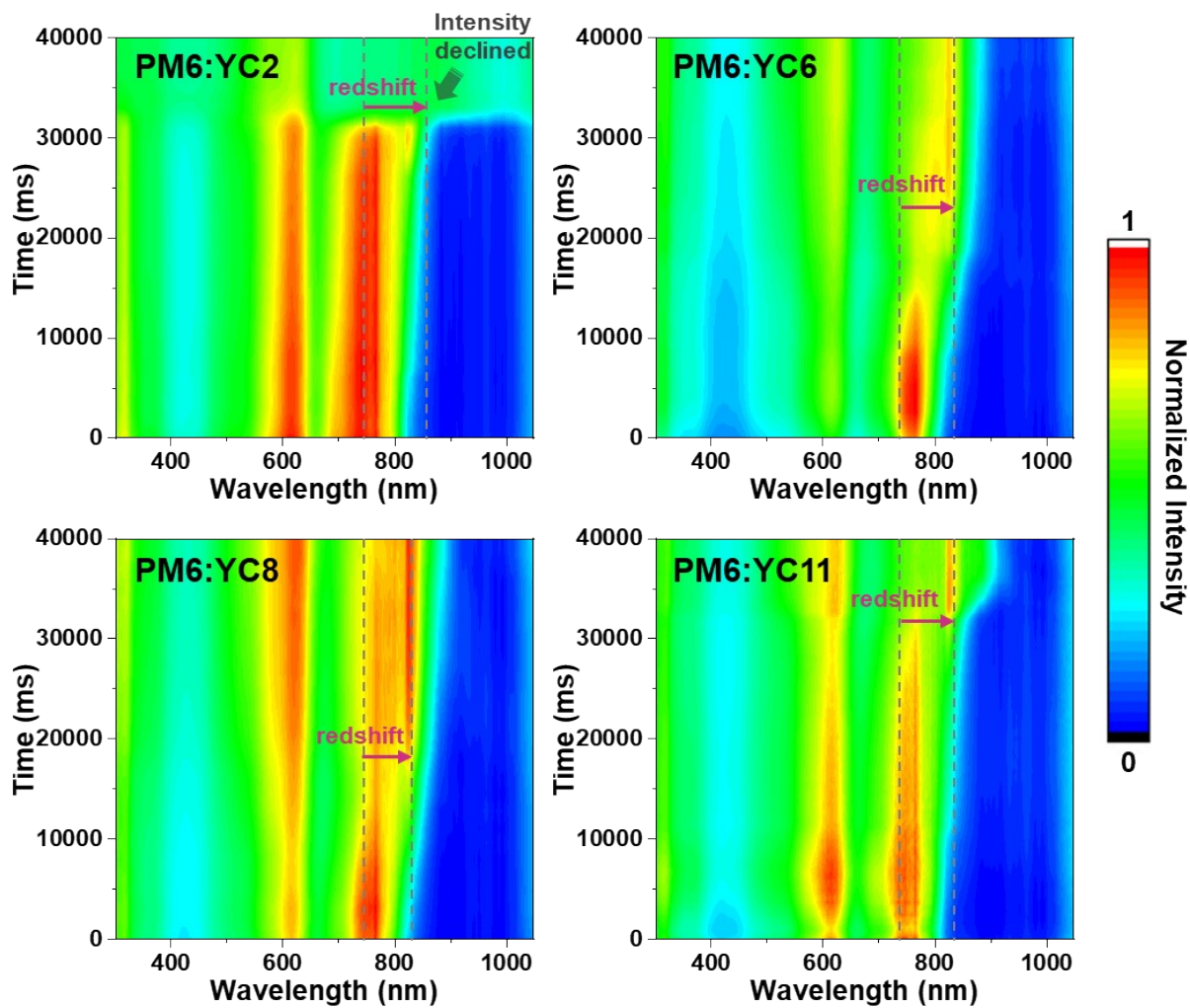
Fig. S29 In situ UV-Vis spectra of blade-coated blends under 20 vol% CB cosolvent condition.
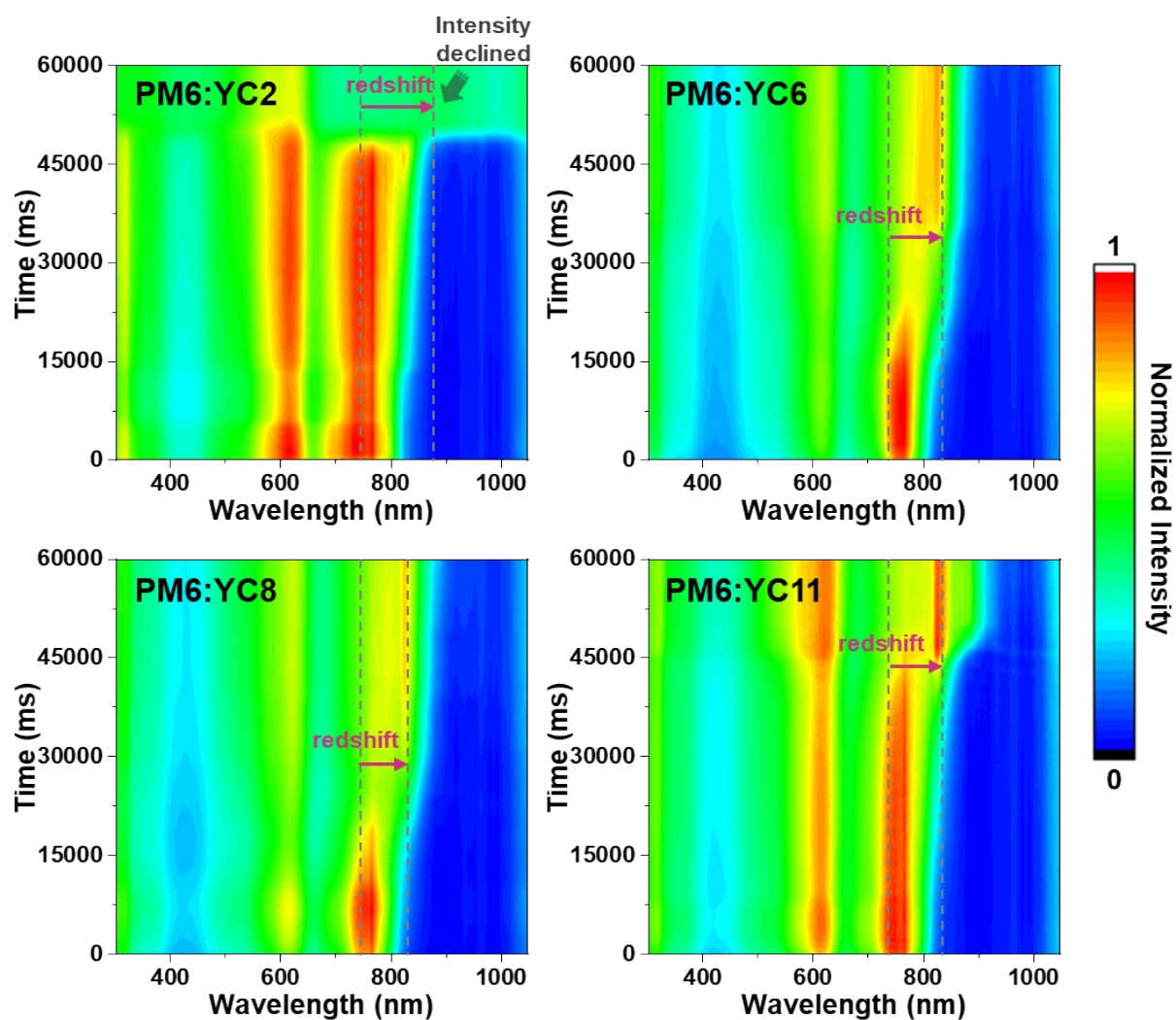
Fig. S30 In situ UV-Vis spectra of blade-coated blends under 30 vol% CB cosolvent condition.
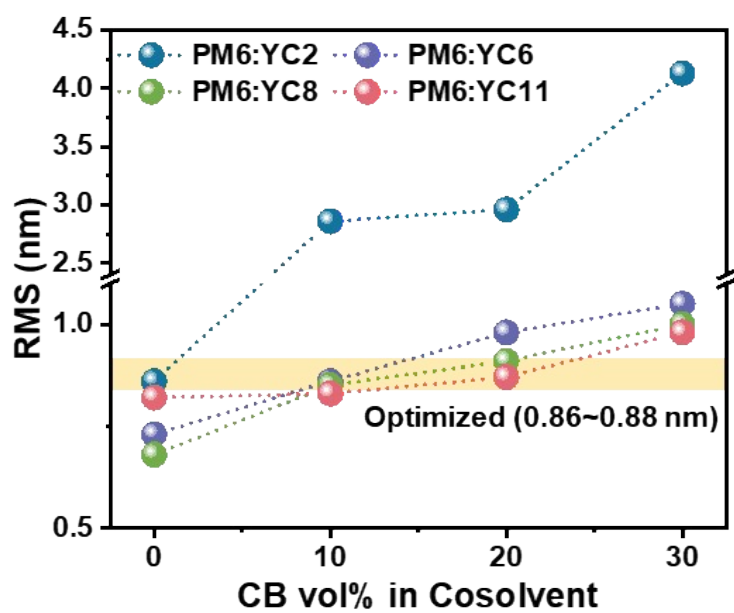
Fig. S31 Comparison of RMS values of blade-coated films fabricated under different cosolvent conditions.
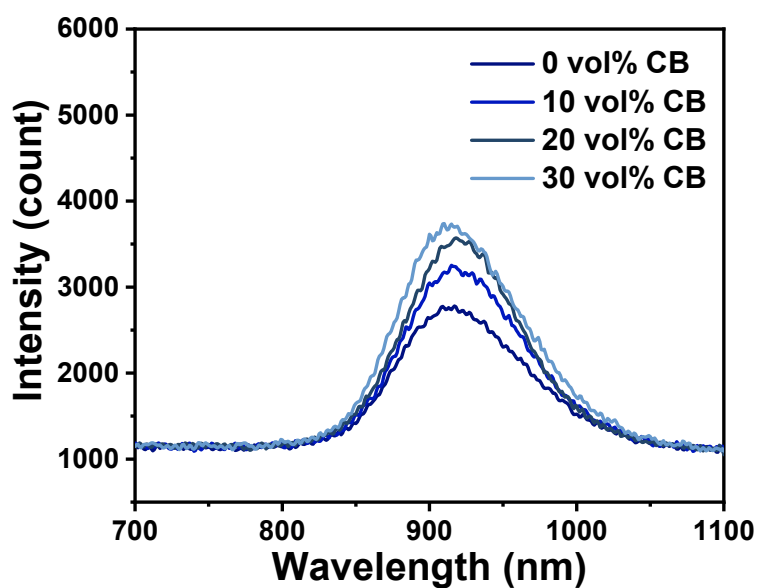
Fig. S32 PL spectra of YC2-based blend films under short-circuit conditions.
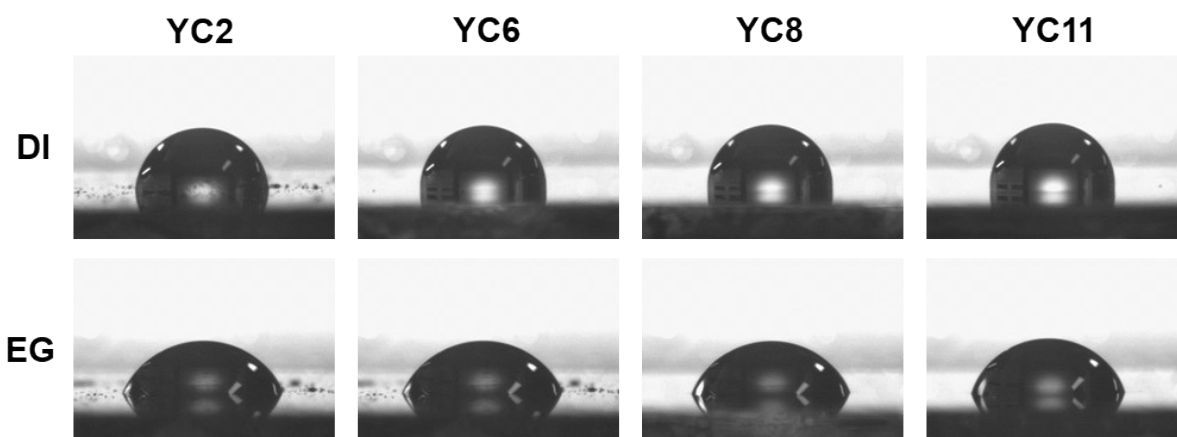
Fig. S33 Contact angle of NFA neat films.

Table S4. Detailed values for contact angle, surface tension, and miscibility parameters of NFAs with PM6.

| Film | Contact Angle | | | | | |
	Θ_{DI} (°)	Θ_{EG} (°)	γ^d (mN m^{-1})	γ^p (mN m^{-1})	Surface tension (mN m^{-1})	χ
YC2	94.4	68.1	17.92	8.92	26.84	0.251
YC6	100.7	69.3	22.42	4.14	26.56	0.225
YC8	101.5	70.1	22.68	3.80	26.48	0.217
YC11	102.9	74.1	20.27	3.83	24.1	0.053
PM6	105.6	78.7	18.41	3.49	21.9	-
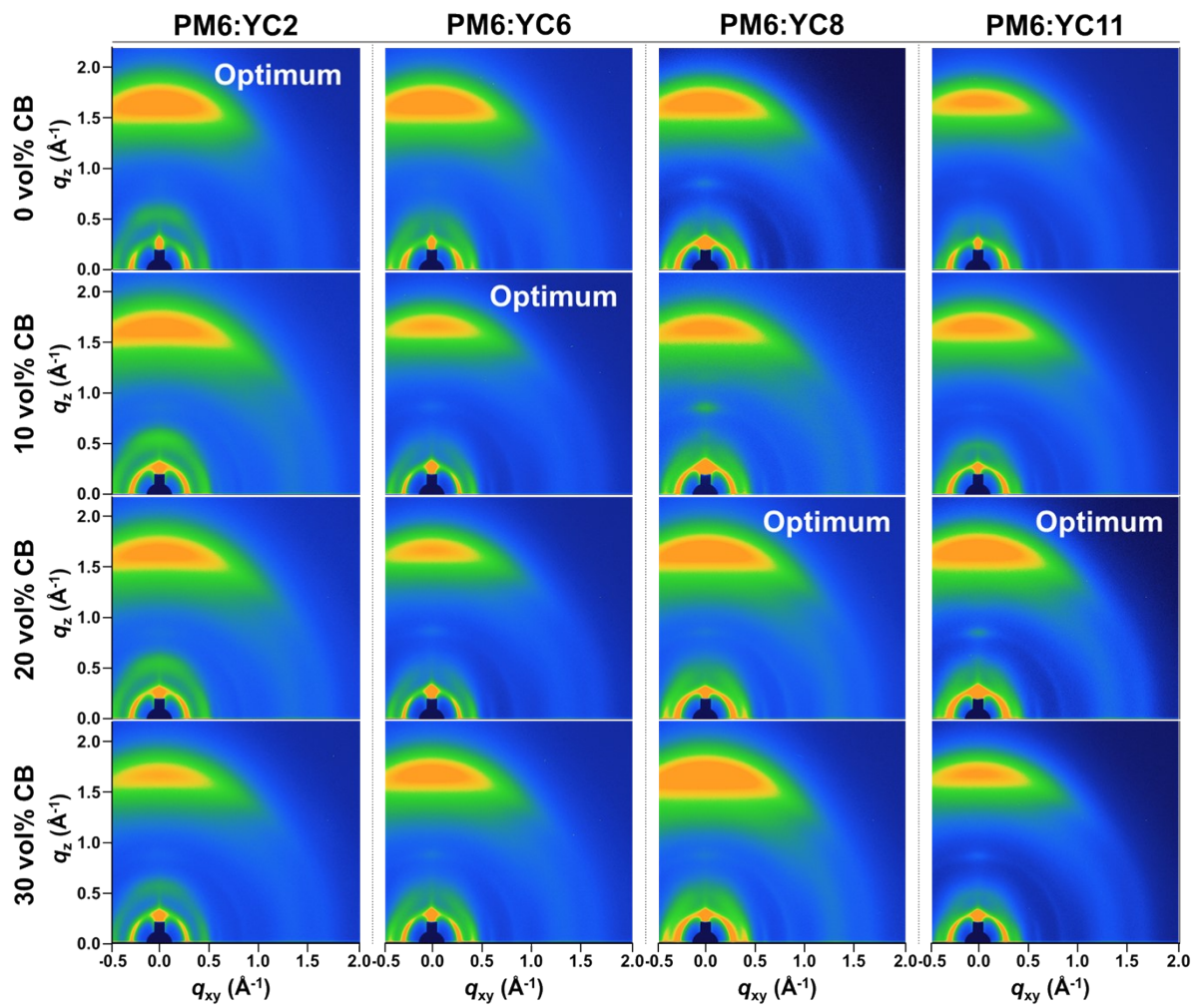
Fig. S34 GIWAXS pattern of blade-coated blend films.
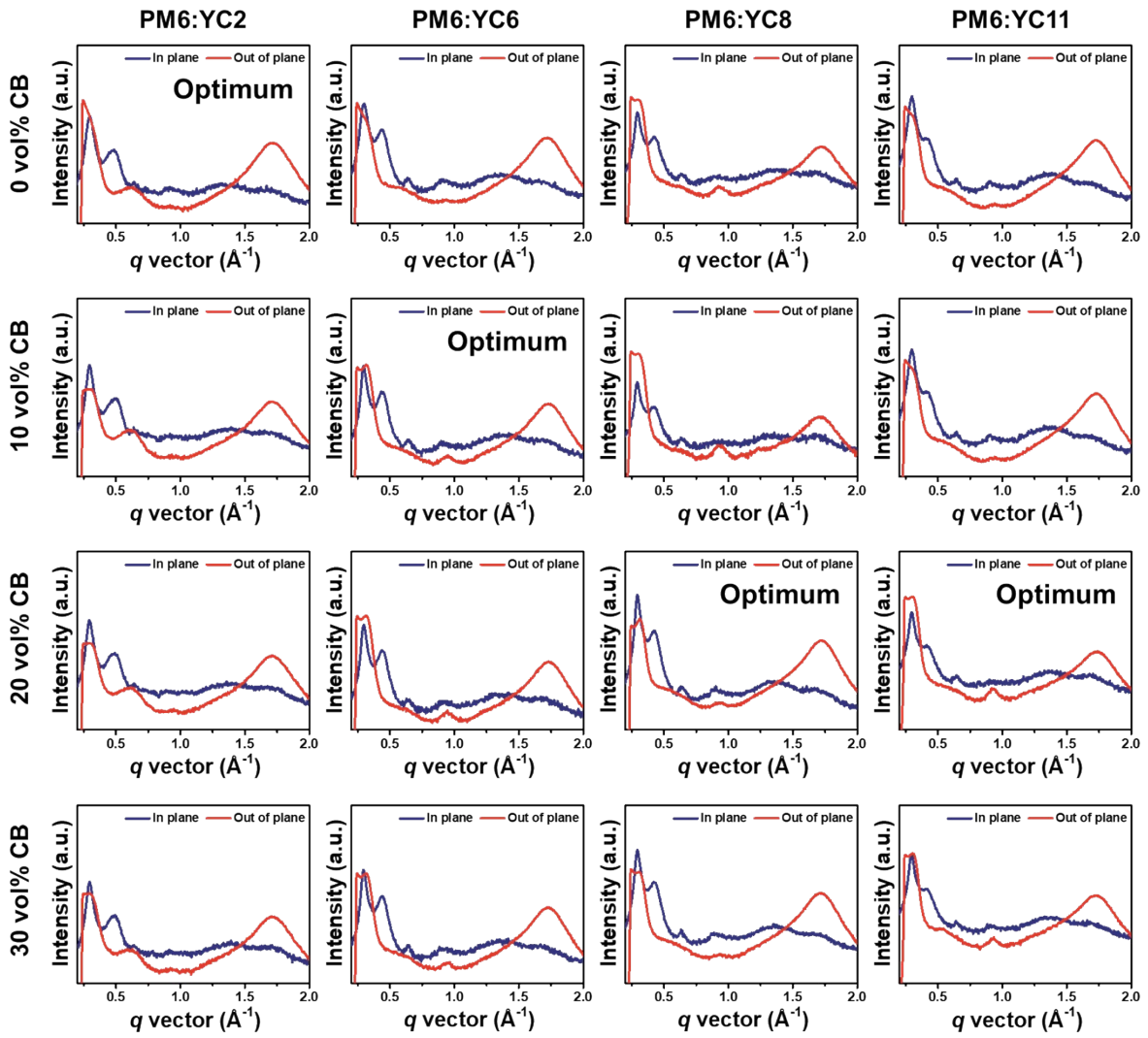
Fig. S35 GIWAXS line cut profiles of blade-coated blend films.

Table S5. Detailed GIWXAS parameters of blade-coated blend films.

| NFA/ CB vol% in cosolvent | Out-of-Plane | | | In-Plane | | | | | |
| | π-π stacking peak | | | [(100)+ (110)] peak | | | (11-1) peak | | |
	q (Å^{-1})	d-spacing (Å)	Coherence length (Å)	q (Å^{-1})	d-spacing (Å)	Coherence length (Å)	q (Å^{-1})	d-spacing (Å)	Coherence length (Å)
YC2/0 vol%	1.71	3.67	25.43	0.30	21.15	113.14	0.49	12.97	69.22
YC2/10 vol%	1.71	3.68	24.49	0.30	21.23	112.93	0.50	12.63	70.07
YC2/20 vol%	1.71	3.68	23.13	0.30	21.25	111.68	0.49	12.80	72.26
YC2/30 vol%	1.71	3.68	23.99	0.30	21.18	114.58	0.49	12.84	75.86
YC6/0 vol%	1.71	3.67	23.91	0.30	21.12	111.16	0.44	14.17	98.25
YC6/10 vol%	1.72	3.65	25.26	0.30	21.18	141.81	0.45	14.12	102.93
YC6/20 vol%	1.72	3.65	25.29	0.30	21.18	138.07	0.45	14.13	103.15
YC6/30 vol%	1.72	3.66	25.91	0.30	21.24	141.53	0.44	14.15	108.83
YC8/0 vol%	1.71	3.67	23.93	0.30	21.27	140.89	0.43	14.52	111.02
YC8/10 vol%	1.71	3.67	24.43	0.30	21.27	150.45	0.43	14.54	112.05
YC8/20 vol%	1.71	3.67	24.83	0.30	21.29	150.33	0.43	14.54	115.77
YC8/30 vol%	1.71	3.67	24.76	0.30	21.32	138.71	0.43	14.50	116.44
YC11/0 vol%	1.72	3.66	23.88	0.30	21.13	94.94	0.41	15.19	64.06
YC11/10 vol%	1.72	3.66	23.94	0.30	21.13	95.09	0.41	15.19	66.76
YC11/20 vol%	1.72	3.65	24.24	0.30	21.16	125.70	0.41	15.30	73.09
YC11/30 vol%	1.72	3.66	24.54	0.30	21.33	127.06	0.41	15.53	73.47
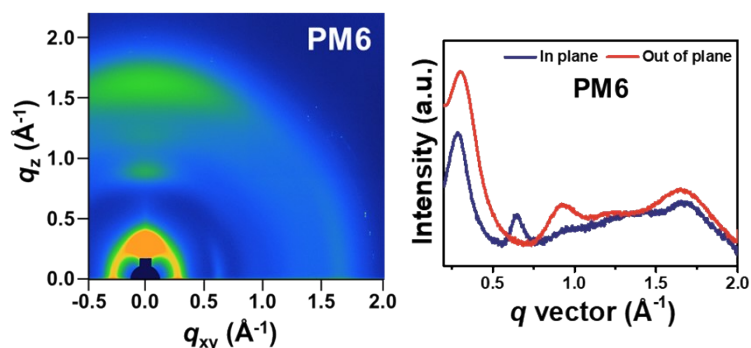
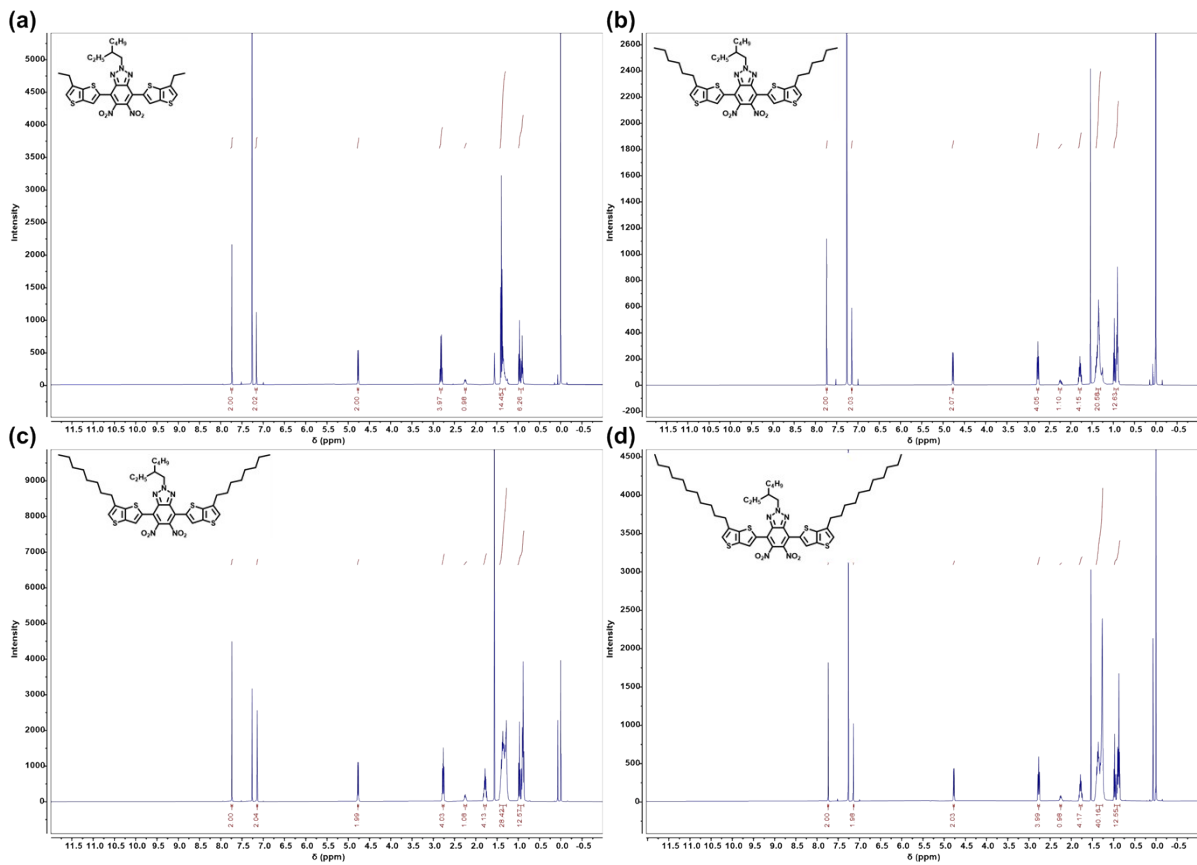**Fig. S36** GIWXAS patterns and corresponding line cut profile of PM6 neat film.

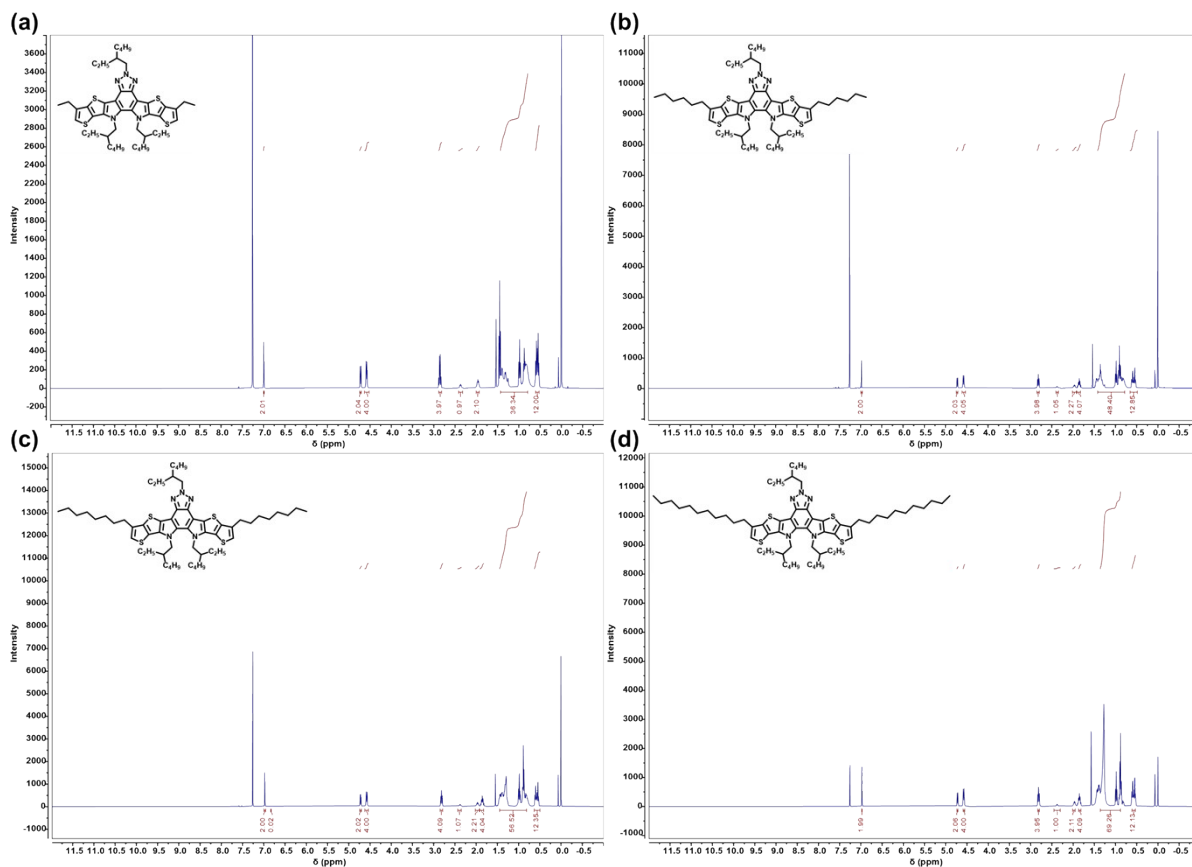**Fig. S37** ^{1}H NMR of (a) **3a**, (b) **3b**, (c) **3c**, and (d) **3d**.

Fig. S38 ^{1}H NMR of (a) **4a**, (b) **4b**, (c) **4c**, and (d) **4d**.
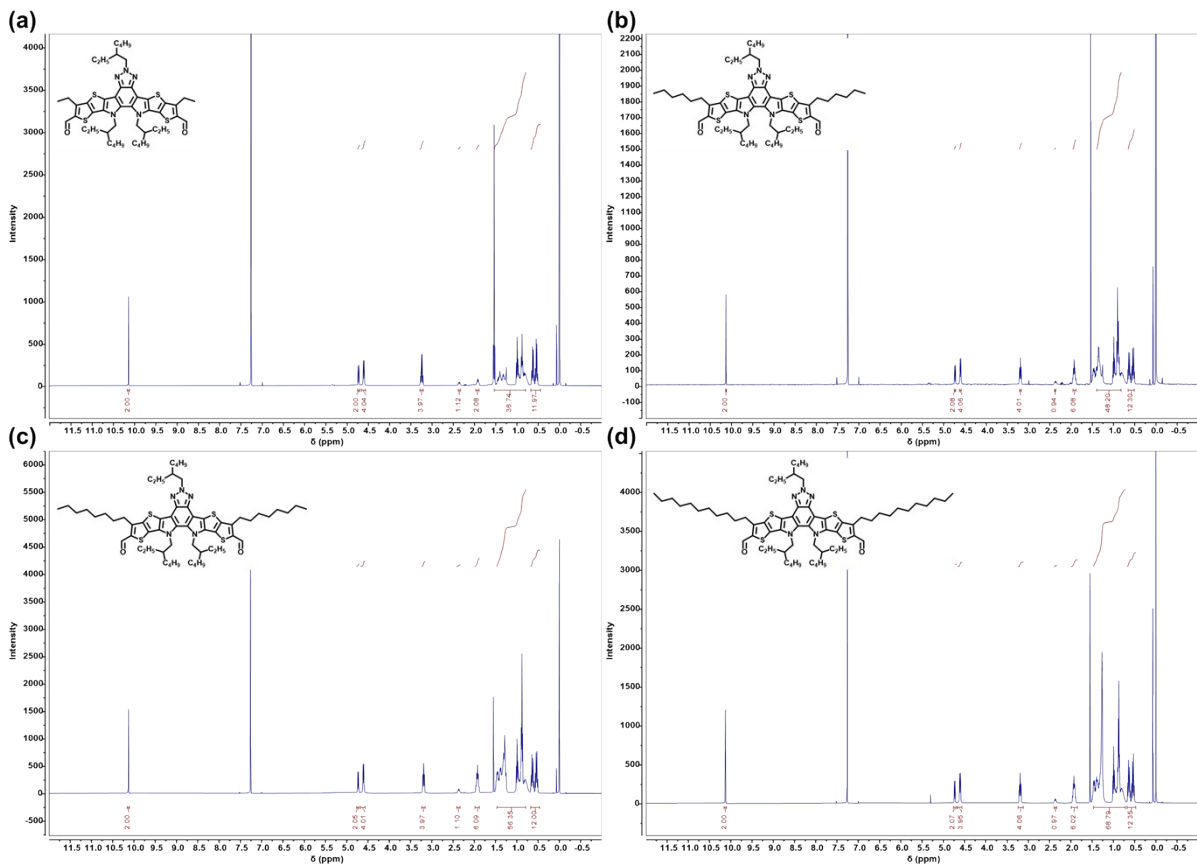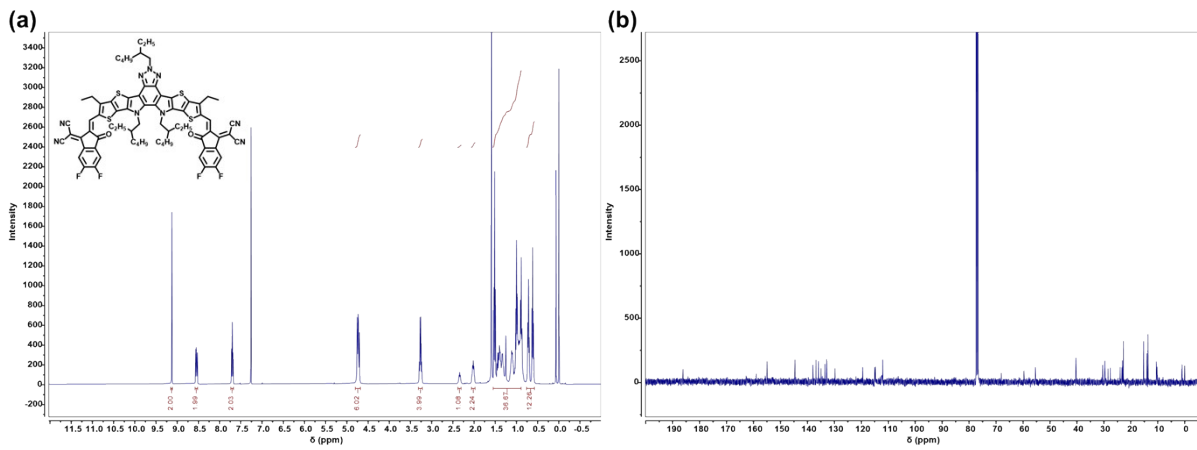
Fig. S39 ^{1}H NMR of (a) **5a**, (b) **5b**, (c) **5c**, and (d) **5d**.

Fig. S40 (a) ^{1}H NMR and (b) ^{13}C NMR of **YC2**.
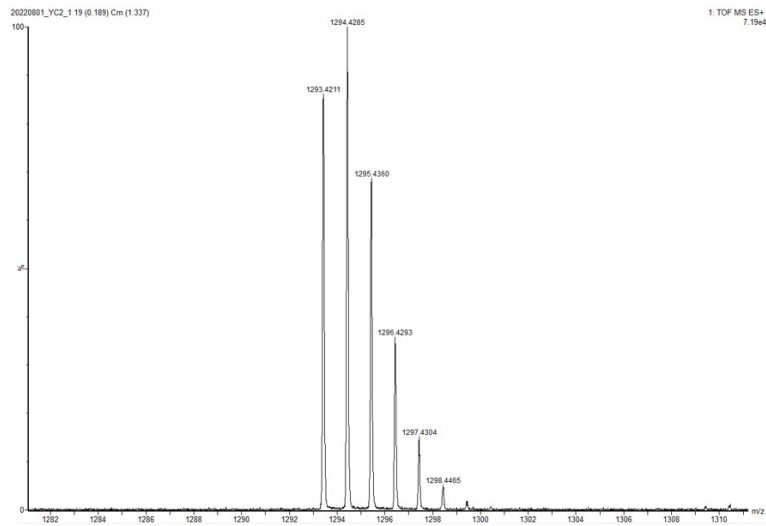
Fig. S41 HRMS spectrum of **YC2**.
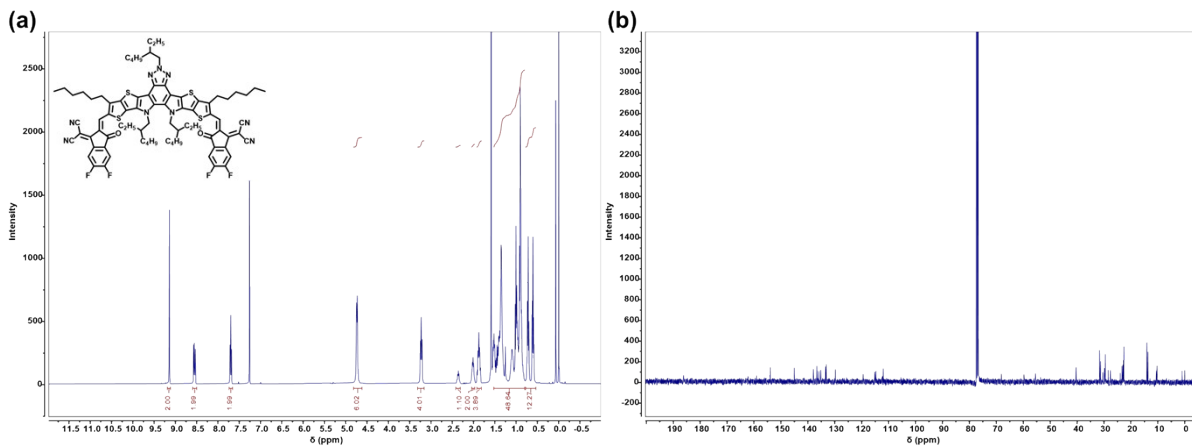
Fig. S42 (a) ^{1}H NMR and (b) ^{13}C NMR of **YC6**.
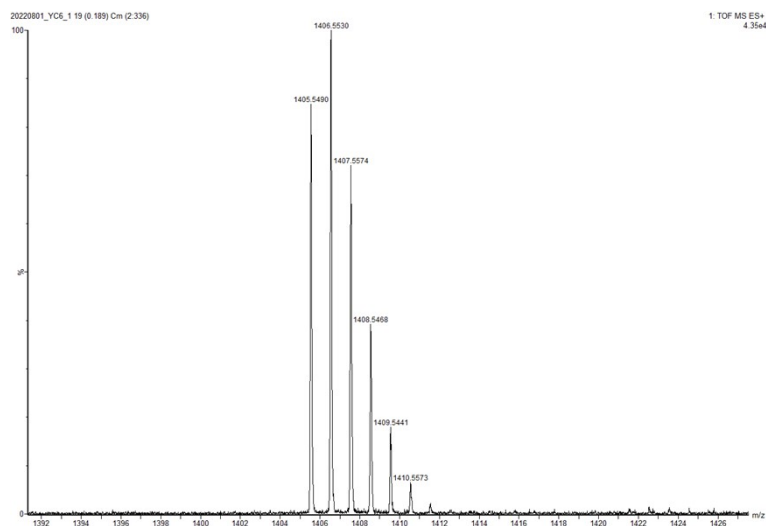
Fig. S43 HRMS spectrum of **YC6**.
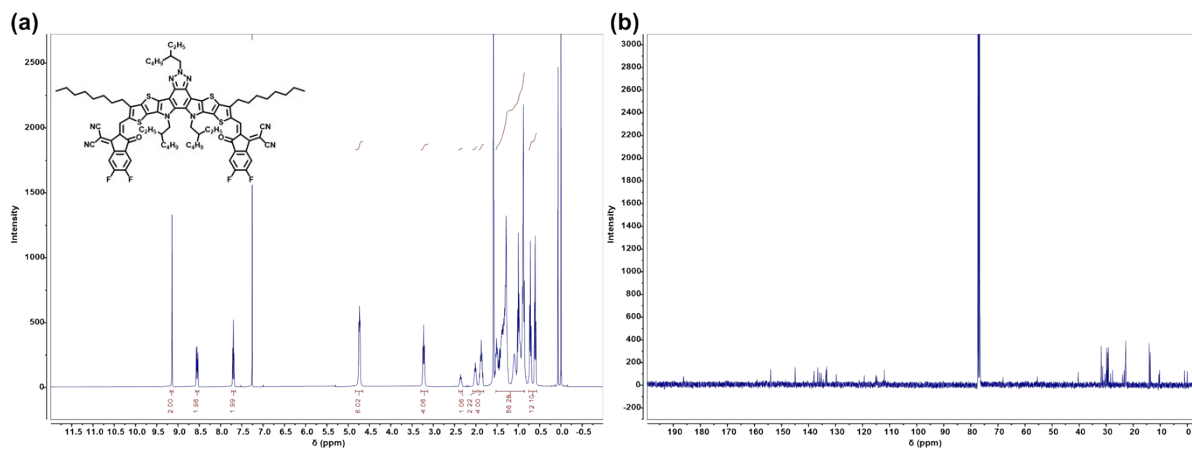
Fig. S44 (a) ^{1}H NMR and (b) ^{13}C NMR of **YC8**.
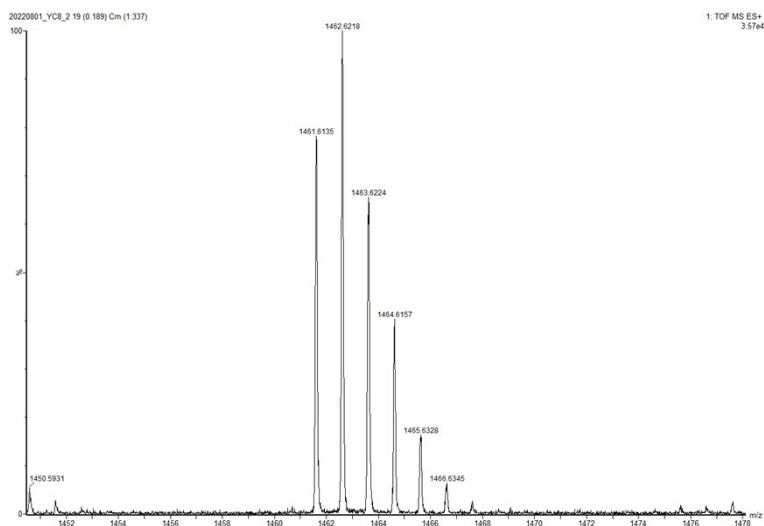
Fig. S45 HRMS spectrum of **YC8**.
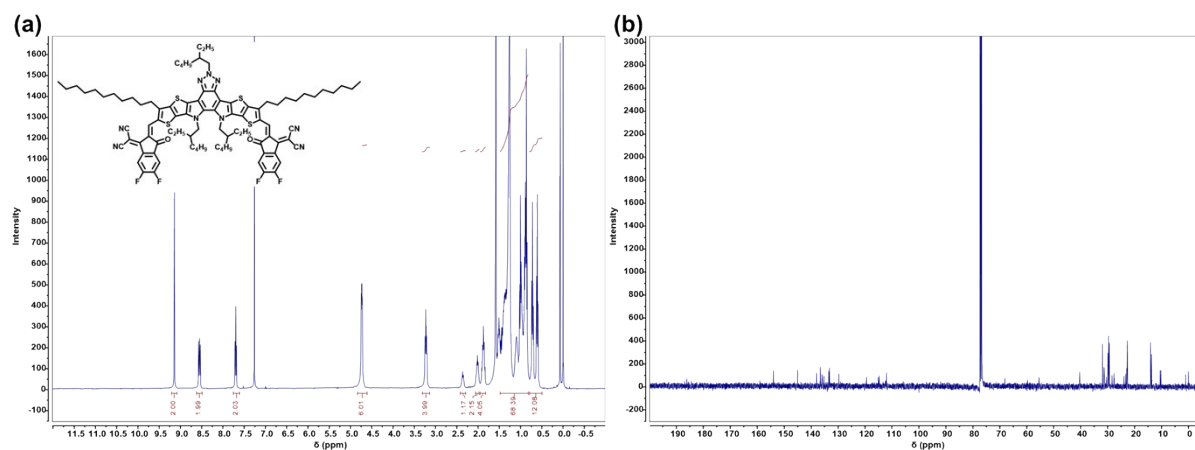
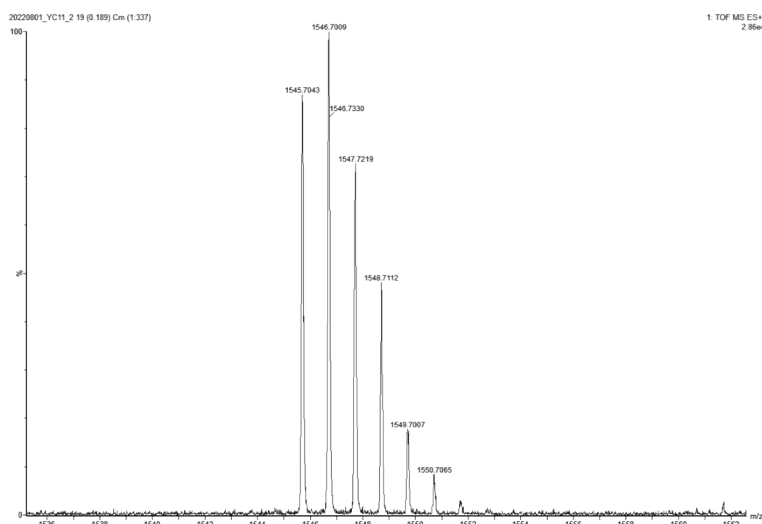**Fig. S46** (a) ^{1}H NMR and (b) ^{13}C NMR of **YC11**.

Fig. S47 HRMS spectrum of **YC11**.

References

1.	C. Zhu, J. Yuan, F. Cai, L. Meng, H. Zhang, H. Chen, J. Li, B. Qiu, H. Peng, S. Chen, Y. Hu, C. Yang, F. Gao, Y. Zou and Y. Li, *Energy Environ. Sci.*, 2020, **13**, 2459-2466.
2.	J. Yuan, Y. Zhang, L. Zhou, G. Zhang, H.-L. Yip, T.-K. Lau, X. Lu, C. Zhu, H. Peng, P. A. Johnson, M. Leclerc, Y. Cao, J. Ulanski, Y. Li and Y. Zou, *Joule*, 2019, **3**, 1140-1151.
3.	T. Jia, W. Zhou, Y. Chen, J. Han, L. Wang, F. Li and Y. Wang, *Journal of Materials Chemistry A*, 2015, **3**, 4547-4554.